I/Q Imbalance Identification and Compensation for Millimeter-wave MIMO Systems

by

Hejir Rashidzadeh

A thesis
presented to the University of Waterloo
in fulfillment of the
thesis requirement for the degree of
Master of Applied Science
in
Electrical Engineering

Waterloo, Ontario, Canada, 2019

Author's Declaration

I hereby declare that I am the sole author of this thesis. This is a true copy of the thesis, including any required final revisions, as accepted by my examiners.

I understand that my thesis may be made electronically available to the public.

Abstract

Today's fourth generation (4G) cellular mobile communication networks are tasked with providing service for an ever increasing number of mobile users and their demand for increased data rates. The fifth generation (5G) of cellular mobile communications will be required to be able to handle the burden currently on 4G networks and also service new technologies as they are introduced. Massive multiple-input multiple-output (MIMO), Millimeter Wave (mmWave) and beamforming have recently been identified as a key enabling technologies for the fifth generation (5G) of cellular mobile communications. Current transmitter typologies exhibit non-idealities that are non-negligible in practical hardware, especially when transmitting wideband mmWave signals. This leads to the requirement that RF building blocks, such as PAs and quadrature modulators, and their respective nonlinearity, and I/Q imbalance must be corrected for.

This thesis proposes a new method to concurrently identify and compensation the I/Q imbalance in mmWave MIMO direct-conversion transmitters (Tx) using a single transmitter observation receiver (TOR). New 5G standards for mm-wave transmitters have strict error vector magnitude (EVM) requirements; however, adjacent channel power ratio (ACPR) requirements are typically relaxed. Therefore, this thesis also proposes judiciously engineered uncorrelated training signals for minimizing the error vector magnitude (EVM) while maintaining acceptable performance in the out-of-band region. The latter is necessary to ensure proper Tx linearization when applying digital predistortion (DPD). The proposed method was validated using a 4 GHz signal in ADS simulation for 1, 2, 4 and 8 Tx chains as well as in measurement using a custom built transmitter comprised of 1, 2 and 4 mm-wave Tx chains utilizing commercially available quadrature modulators. NMSEs of 19.9% before and 2.25% after I/Q imbalance compensation were obtained. Finally, the compensation accuracy of the proposed method was further confirmed when the I/Q compensation filters are calculated in back-off and applied during the DPD linearization of a mm-wave power amplifier (PA).

Acknowledgements

I would like to thank my supervisor Dr. Boumaiza for his guidance throughout my Masters. I would also like to thank Dr. Mitran for his insight and advice during the process of completing my work. Finally, I would like to thank another member of the EmRG research group, Mohammed Almoneer, who shared his knowledge with me, showed me many resources to learn from and helped me learn the ropes of how research was conducted. This work could not have been done without these people.

Dedication

This thesis is dedicated to my mother, my father and the rest of my family members who have helped me throughout this journey.

Table of Contents

List of Tables

List of Figures

Abbreviations

3G third generation 10

3GPP 3rd Generation Partnership Project 7

4G fourth generation 1, 10

5G fifth generation 1, 2, 4, 7, 12, 13, 18

ACPR adjacent channel power ratio 1, 13, 27, 35–37, 43

CRV complexity-reduced Volterra 43

DAC digital-to-analog converter 2, 4

DPD digital predistortion 7, 10, 11, 13, 18–20, 27, 35, 43

EVM error vector magnitude 1, 7, 13, 27, 35, 36, 43

FIR finite impulse response 22, 29

IIR infinite impulse response 26

IOT Internet of Things 1

LO local oscillator 6, 7, 40

MIMO multiple-input multiple-output 1–3, 12, 18, 20–22, 37, 38

mmWave millimetre wave viii, 1–3, 12, 13, 16, 21, 35, 43

MSE mean squared error 28, 30, 32

NMSE normalized mean squared error 7, 36–38, 42

PA power amplifier 19, 20, 27, 35, 43

PSD Power Spectral Density 27, 28, 31, 34–37

RF radio frequency 21, 27, 40

SISO single input and single output 1, 4, 10, 18

SMDA spacial division multiple access 2, 12, 17

TOR transmitter observation receiver 18, 20, 21, 24, 35, 36, 38, 42

Tx transmitter 22

UWB ultra wideband 1, 2, 4, 13, 18

List of Symbols

$Im\{\cdot\}$ Imaginary operator: denotes the imaginary component of a complex signals.

$Re\{\cdot\}$ Real operator: denotes the real component of a complex signals.

x Complex scalar: denoted in lowercase.

$\boldsymbol{x}$ Complex vector: represents a vector of complex scalars, i.e., $[x(0), x(1), \cdots, x(N)]^T$ denoted in bold lowercase.

$\boldsymbol{X}$ Complex matrix: represents a matrix of complex scalars denoted in bold uppercase.

$H(z)$ Z-domain expression: denotes the z-transform of the impluse response h(n).

$I_{N\times N}$ Identity matrix: denotes the identity matrix of size $N \times N$.

$\|\cdot\|^2$ L^2 norm: denotes the L^2 norm of a vector

Chapter 1

Introduction

Today's fourth generation (4G) cellular mobile communication networks are tasked with the heavy burden of the ever increasing number of mobile users and their demand for data faster data rates. As new technologies are introduced, the fifth generation (5G) of cellular mobile communications will be required to manage enormous speeds to multiple times more devices than 4G cellular networks. There are 5 technologies leading the way in enabling the first 5G networks. These are mmWave, massive multiple-input multiple-output (MIMO), beamforming, small cells, and full duplex [1], [2]. This thesis focuses on identifying and compensating for transmitter hardware impairments in mmWave quadrature modulators modulators for MIMO systems. The transition from sub 6GHz and single input and single output (SISO) systems to mmWave and MIMO brings a new set of challenges that must be carefully considered when finding a solution to compensating for hardware impairments in upcoming 5G systems.

As technologies such as smart vehicles, smart transport and the Internet of Thingss (IOTs) become a reality, the need for bandwidth and available spectra increase. The current sub-6GHz frequency bands used for mobile communications do not have enough bandwidth to support all emerging applications [1]. As a result, future 5G systems will utilize the mmWave frequency bands, enabling ultra wideband (UWB) signal transmission. Furthermore, new 5G standards for mmWave transmitters have strict error vector magnitude (EVM) requirements; however, adjacent channel power ratio (ACPR) requirements

are typically relaxed [3]. Therefore, with the move to 5G careful consideration should be taken when deciding the signals that are used to identify and compensate for the transmitter hardware impairments.

Both massive MIMO systems and beamforming can be classified as MIMO technologies, and their similarities lie in the fact that they both utilize multiple transmitter chains, albeit, for different purposes. Massive MIMO refers to the transmission of multiple data streams simultaneously to multiple different users using spacial division multiple access (SMDA). Massive MIMO are equally essential for sub$4-36$GHz and mmWave 5G systems [4]. The use of multiple transmitter chains in massive MIMO leads to an accumulation of the non-idealities caused by hardware impairments in each transmitter chain. This issue is compounded even further as the number of transmitter chains increases. On the other hand, beamforming uses antenna arrays to transmit signals by focusing beams in a specific direction. There are three main methods of beamforming: digital beamforming, where each antenna is fed by an independent transmitter, RF beamforming, where one transmitter feeds multiple antennas, and finally hybrid beamforming which is a combination of both previous types of beamforming [5]. Similarly, the use of multiple transmitter chains in beamforming one again leads to an accumulation of the non-idealities caused by hardware in each transmitter chain. Accordingly, with the move to multiple transmitter systems, compensation schemes should find efficient ways to compensate for compounded impairments efficiently and simultaneously.

Current transmitter topologies either utilize direct upconversion using quadrature modulation or two step generation where the signals are generated at IF using RF digital-to-analog converters (DACs) and upconverted to RF frequencies with a mixer. Quadrature modulators are preferable to other methods of generating UWB RF signals as the sampling rate requirement is halved compared to using a DAC to generate the complex signal at IF [6]. Using quadrature modulators also lowers the RF bandwidth requirement on the DAC. However, quadrature modulators have inherent non-idealities that must be compensated for. As outlined above, with the advent of new 5G technologies, first careful consideration must be taken when considering the signals used to identify transmitter nonidealities and a method of compensation must be developed that can efficiently handle the compounding nonidealities caused by the multiple transmitters in massive MIMO and beamforming

systems.

This thesis is organized into the following chapters, First, in Chapter 2, the background theory on quadrature modulators and their inherent I/Q imbalance is presented, this is followed by a literature review of the current I/Q compensation schemes. Afterwords, a literature review of current 5G technologies is demonstrated. Chapter 2 ends with the background and literature review of I/Q imbalance compensation schemes in MIMO systems. Chapter 3 presents the proposed method of compensating transmitter I/Q imbalance in mmWave MIMO systems as well as judiciously engineered training signals to be used in the identification process. This chapter ends by validation of the method and training signal in both simulation and measurement. Lastly, Chapter 4 outlines the conclusion and the possible avenues for future work to be conducted.

Chapter 2

Background Theory

2.1 I/Q Imbalance in SISO Systems

In this section we begin by outlining the basics of I/Q imbalance effects in SISO systems and an overview of the literature on methods of I/Q imbalance identification and compensation are presented.

2.1.1 Overview of I/Q Imbalance

Quadrature modulators are used to generate complex signals at RF frequencies. Quadrature modulation are preferable to other methods of generating UWB RF signals as the data streams are split into separate in-phase (real) and quadrature-phase (imaginary) components. Therefore, the sampling rate requirement on the DACs is halved compared to using a DAC to generate the complex signal at IF [6], which would then be up-converted to RF frequencies by a mixer. Using quadrature modulators also lowers the RF bandwidth requirement on the DAC. Therefore despite the introduction of RFDACs the ever increasing bandwidth requirements for 5G systems means quadrature modulators are still readily used to generate UWB signals.

Lets say we have a generic complex signal [7] that we want to generate, as shown in

Fig. 2.1. This signal can be represented in rectangular form as,

$$\tilde{x}(t) = x_I(t) + jx_Q(t) \tag{2.1}$$

This signal can also be represented in polar form as,

$$\tilde{x}(t) = |\tilde{x}(t)|e^{j\theta(t)} \tag{2.2}$$

where

$$|\tilde{x}(t)| = \sqrt{x_I^2(t) + x_Q^2(t)}$$

$$\theta(t) = tan^{-1}\left(\frac{x_Q(t)}{x_I(t)}\right)$$

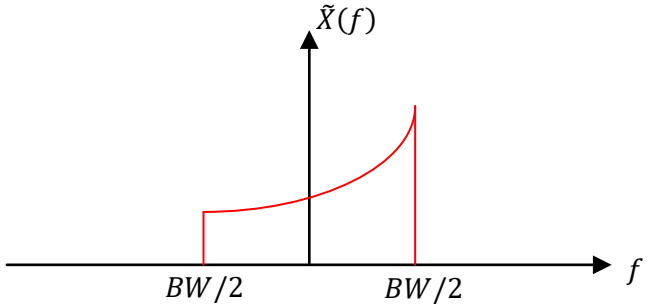

Figure 2.1: Generic complex signal to be generated.

Of course we cannot generate this signal at baseband since it is a complex signal. To generate this signal, we must do so using an RF carrier, i.e.,

$$\begin{aligned} x_{RF}(t) &= Re[\tilde{x}(t)e^{j2\pi f_c t}] \\ &= Re[\,|\tilde{x}(t)|e^{j\theta(t)}e^{j2\pi f_c t}] \\ &= Re[\,(x_I(t) + jx_Q(t))e^{j2\pi f_c t}] \\ &= Re[\,(x_I(t) + jx_Q(t))(cos2\pi f_c t + jsin2\pi f_c t)] \\ x_{RF}(t) &= x_I(t)cos2\pi f_c t - x_Q(t)sin2\pi f_c t \end{aligned} \tag{2.3}$$

The block diagram of a quadrature modulator is shown in Fig. 2.2, it can be seen that it preforms the operation shown in (2.3). In order to see the operation of quadrature modulator clearly, it is best to demonstrate the operation in the frequency domain as shown in Fig. 2.3. It can be seen that the real ($X(f)$) and imaginary ($X(f)$) signals are combined into the original complex signal at the desired RF frequency. This operation is dependent on the ability of the physical quadrature modulator to emulate this ideal behaviour.

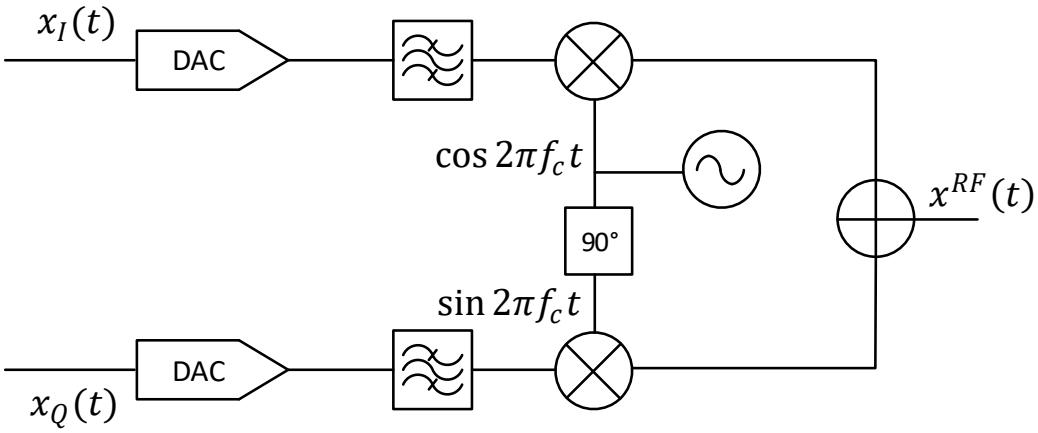

Figure 2.2: Block diagram of a quadrature modulator.

I/Q imbalance is detrimental to the ideal RF signal generation displayed in Fig. 2.3. I/Q imbalance arises from the physical components non-idealities and can be categorized into two effects. First, ideally, the I and Q paths must have identical phase and amplitude response which do not vary with frequency. In reality, however, this is not the case, and the amplitude and phase imbalance leads to improper combining of the I and Q components of the signal. Second, the hybrid 90° coupler used to drive the mixers with the local oscillator (LO) signals might not have perfect 90° phase offset between the two output ports meaning the I and Q components will not be mixed with the proper $cos2\pi f_c t$ and $sin2\pi f_c t$ carriers. Once again, this offset will lead to non-ideal combining.

Fig. 2.4 displays the behaviour a physical quadrature modulator exhibits when it exhibits I/Q imbalance. In this example, instead of perfect 90° phase difference between the two paths, the phase difference is 80°, causing a 10° phase imbalance. There is also

an amplitude imbalance between the two paths with the I path having 3dB attenuation compared to the Q path. Due to this I/Q imbalance we have unwanted gray and gray dotted imaginary components in the up-converted signal shown in Fig. 2.4(e). We also see that the real components have not cancelled properly with a red dashed residual signal on the negative real axis. Clearly, without perfect amplitude and phase and balance between the paths, there is a severe degradation in signal quality. In a practical RF system this translates to high EVM or normalized mean squared error (NMSE), for which there are stringent requirements in new 3rd Generation Partnership Project (3GPP) 5G standards [3]. Therefore, in the literature, I/Q imbalance compensation techniques have received significant attention.

2.1.2 Literature Review

In the literature, most I/Q imbalance identification and compensation schemes can be divided into three categories. Frequency independent, frequency dependent and joint I/Q imbalance and digital predistortion (DPD) compensation schemes.

Frequency Independent

Frequency Independent I/Q imbalance compensation schemes consider the I/Q imbalance to be a constant amplitude and phase offset that does not vary with frequency. Frequency independent I/Q imbalance effects are sometimes referred to as static I/Q imbalance. The authors in [8] analyze the static I/Q imbalance effects and provides a quantitative assessment of the losses. The authors then present adaptive compensation techniques for the quadrature modulator at both the transmitter and receiver. Similarly, the authors in [9] present an adaptive I/Q imbalance compensator which estimates and separates the respective I/Q imbalances of the transmitter and receiver by utilizing a 90° shift in the LO. These solutions are feasible in systems with smaller modulation bandwidths. As the data rates of systems increases, leading to larger modulation bandwidths frequency independent I/Q imbalance compensation schemes become ever more impractical.

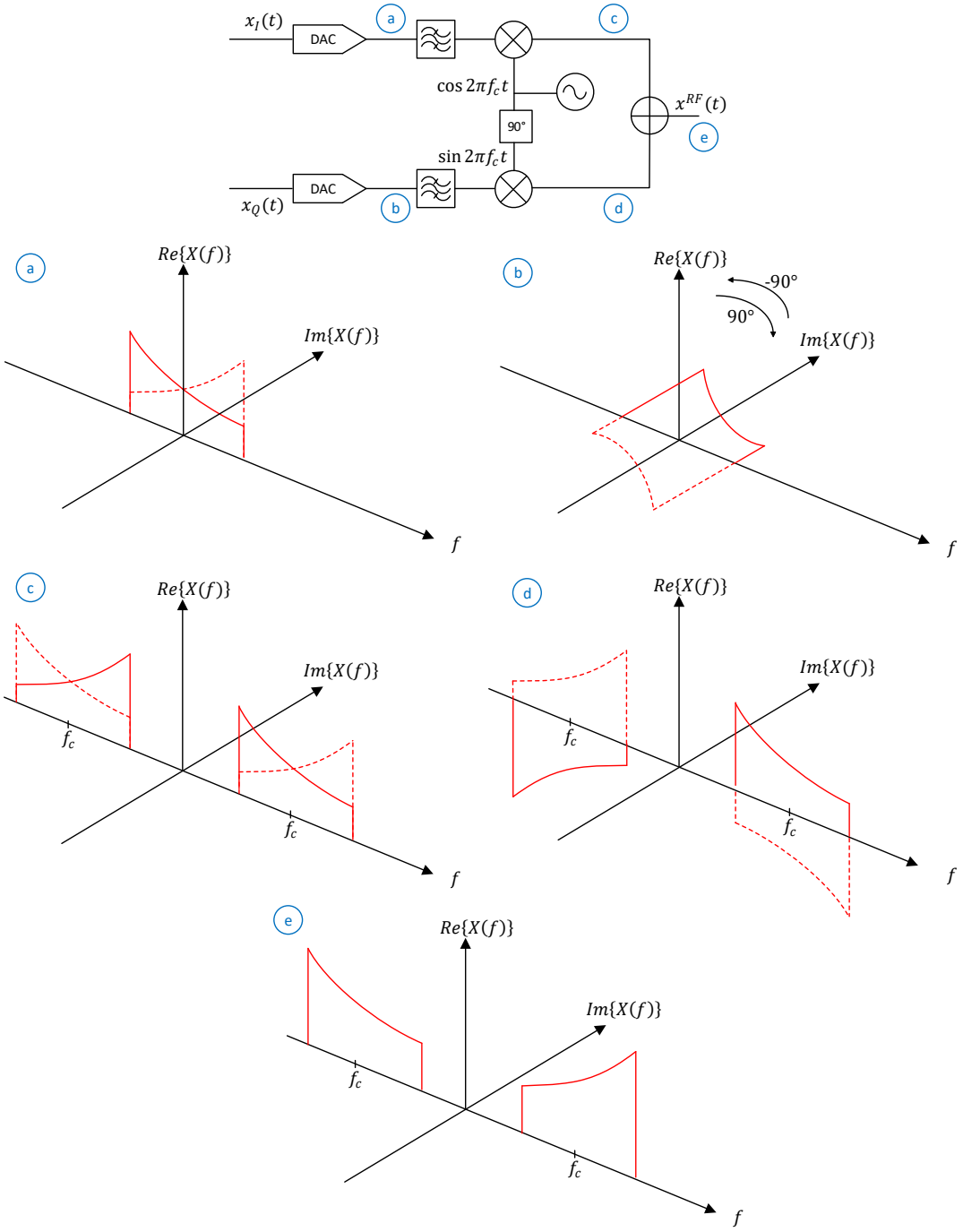

Figure 2.3: Ideal Quadrature modulation to generate signals at RF frequencies.

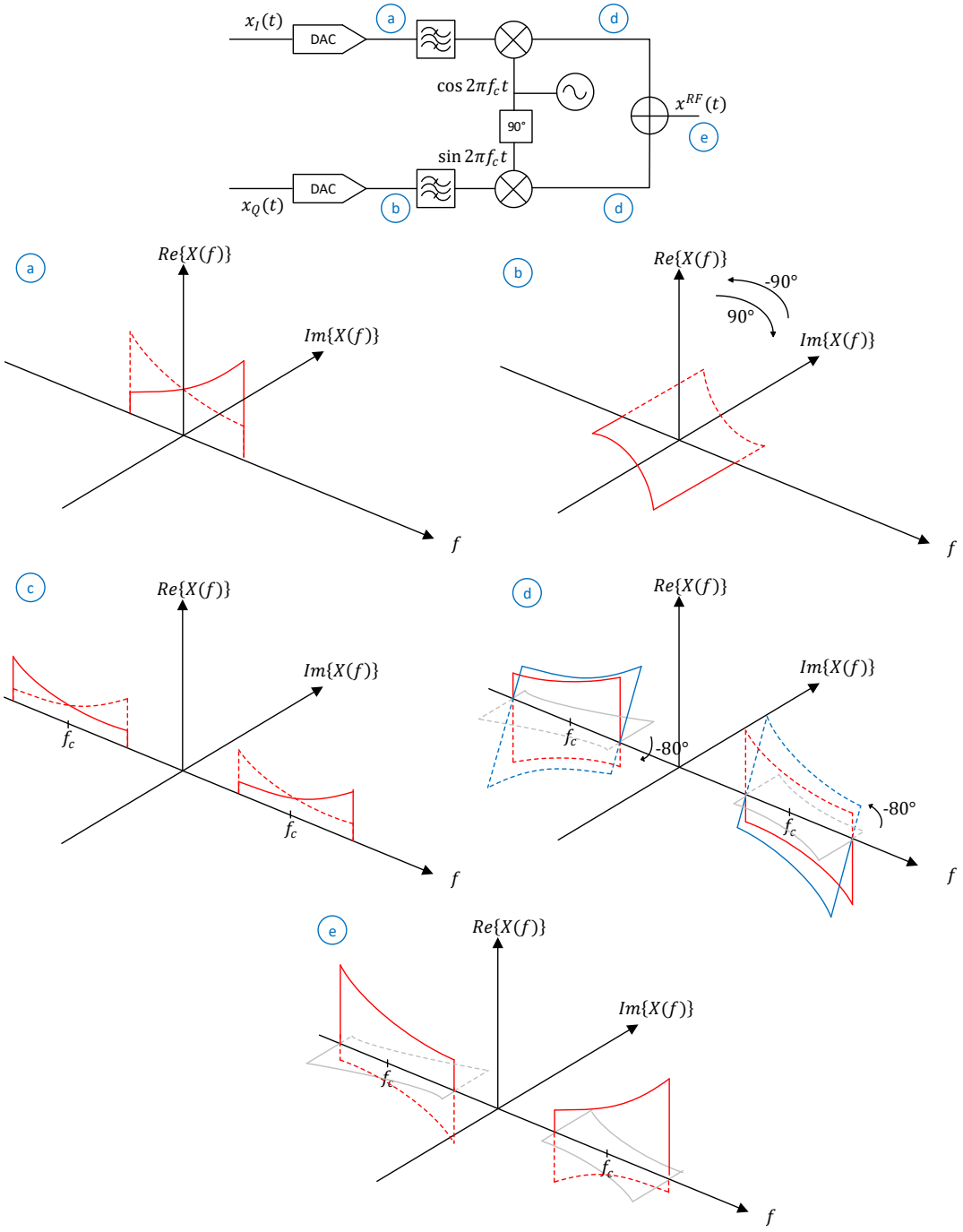

Figure 2.4: Quadrature modulation with I/Q imbalance when generating RF frequencies

Frequency Dependent

Third generation (3G) and 4G systems brought with them higher data rates and therefore used greater modulation bandwidths to transmit signals. As the modulation bandwidth increases beyond a few MHz frequency-dependent I/Q imbalance effects become more important. It is no longer feasible to model the I/Q imbalance as a simple amplitude and phase offset.

SISO I/Q imbalance compensation techniques have received significant attention [10], [11], [12], [13]. The first comprehensive model for I/Q imbalance was presented in [10] for quadrature IF radio receivers. The model, shown in Fig. 2.5, and covered in extensive detail in Chapter 3, approximates the quadrature modulator as four real-valued FIR filters. This model is adopted in [11] and [12] for transmitters. In [11] the authors use a least-squares based time domain approach to identify and compensate for the I/Q imbalance. While the authors in [12] take a frequency domain approach and take advantage of the aliasing exhibited during sub-sampling in combination with multi-tone training signals to reduce the sampling rate during I/Q imbalance identification.The authors in [13] assume a similar model, shown in Fig. 2.6. However, when it came to compensation they only compensate for the effects of H_2. The authors also present two estimation approaches, the first estimation approach stems from second-order statistics of complex communication signals, while the second technique is based on widely-linear least-squares model fitting.

These approaches cannot be directly generalized to large-scale MIMO systems. In fact, the increase in the number of quadrature modulators in MIMO systems brings a new set of challenges and trade-offs. Especially when considering that the I/Q imbalance not only deteriorates the error vector magnitude (EVM) of the output signal but is also detrimental to the linearization of PAs using DPD [6].

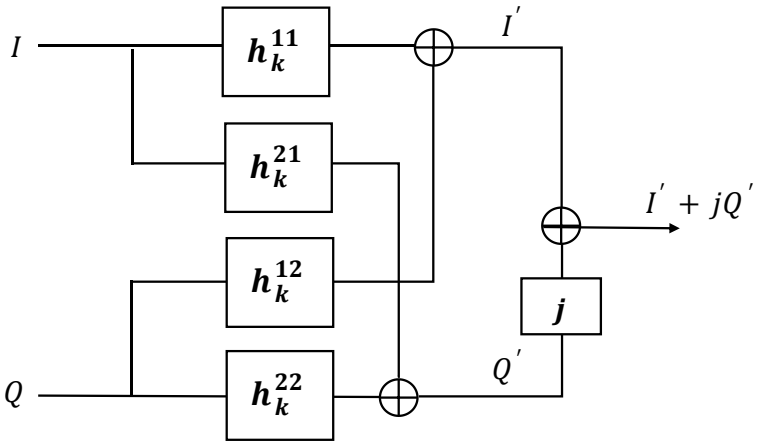

Figure 2.5: Block diagram of the baseband model of a quadrature modulator.

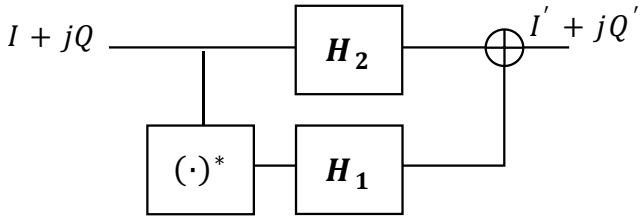

Figure 2.6: Block diagram of the baseband model of a quadrature modulator.

Joint I/Q and DPD

In an effort to alleviate transmitters of both linear and nonlinear impairments. Many publications propose joint I/Q imbalance and DPD compensation schemes. These include extending the parallel Hammerstein structure [14], Volterra series model [15] and asymmetrical complexity-reduced Volterra series (CRV) model [16]. These methods, although compact, suffer from an increase in computational complexity compared to independent I/Q compensation. This occurs because when any linear memory is present before the non-linearity it significantly increases the linear memory order required in the DPD [17] [18]. Overall, resulting in an exponential increase in the number of DPD coefficients needed to compensate the combined nonlinearity and I/Q imbalance.

2.2 5G Technologies

Although 5G systems are still in their early stages of development, 5 technologies have emerged as front-runners in realizing 5G wireless networks [2]. These are mmWave, massive MIMO, beamforming, small cells, and full duplex.

Massive MIMO and beamforming can both be categorized as subsets of MIMO systems. MIMO simply stands for mulitple-input multiple-output, which on the transmitter side indicates the use of multiple transmitter chains. The difference between massive MIMO and beamforming can be summarized as follows, beamforming uses antenna arrays to transmit signals by focusing beams in a specific direction. In contrast, massive MIMO refers to the transmission of multiple data streams simultaneously to multiple different users using SMDA.

This thesis tackles the problem of I/Q imbalance in mmWave MIMO systems. Therefore, in this section, a brief summary and literature review of mmWave, massive MIMO and beamforming systems demonstrates how the addition of multiple transmitter chains, and the specific architectures used in new 5G systems brings a new set of challenges and trade-offs when correcting for transmitter hardware impairments, and specifically for our case, I/Q imbalance.

2.2.1 Millimeter Wave

As today's cellular providers attempt to deliver higher data rates to an ever increasing number of users, they are limited to the frequency spectrum range below 6GHz [1]. One way to keep up with the demand is to move to the mmWave frequencies. There are various definitions of the frequencies that are considered to be the mmWave. However, most articles consider the mmWave band to be between 24GHz and 300GHz [19], [20], [1], [21], [2]. Early research focused on the lower ends of mmWave frequencies due to atmospheric absorption characteristics at frequencies such as 28GHz and 38GHz as can be seen in Fig.2.7 [1]. As a result, the FCC recently auctioned off the 24GHz and 28GHz mmWave spectrum in early 2019.

Moving to the mmWave frequencies opens a new portion of the spectrum for new signals. As a result of the new-found availability of spectra, transmitters will be using larger modulation bandwidths in order to provide higher data rates [21], [1]. As a result, frequency dependent I/Q imbalance impairments will be more important than ever. Therefore, any future I/Q imbalance identification and compensation schemes must be able to withstand the large variations of hardware behavior over bandwidths in the 100s of MHz exhibited by UWB signals. Moreover, new 5G standards for mmWave transmitters have strict EVM requirements; however, ACPR requirements are typically relaxed [3]. Therefore, with the move to 5G careful consideration should be taken when deciding the signals that are used to identify and compensate for the transmitter hardware impairments. These signals should prioritize the EVM minimization over ACPR minimization when applying DPD.

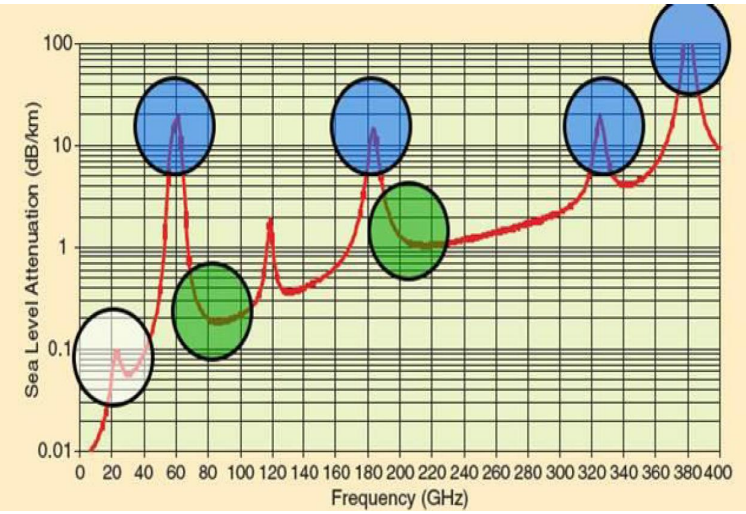

Figure 2.7: Atmospheric absorption at different frequencies [1].

2.2.2 Beamforming

Beamforming uses antenna arrays to transmit signals by focusing beams in a specific direction. There are three main methods of beamforming: digital beamforming, where each antenna is fed by an independent transmitter, RF beamforming, where one transmitter

feeds multiple antennas, and finally hybrid beamforming which is a combination of both previous types of beamforming [5]. Each beamforming architecture has its benefits and drawbacks, therefore they are utilized for applications[22].

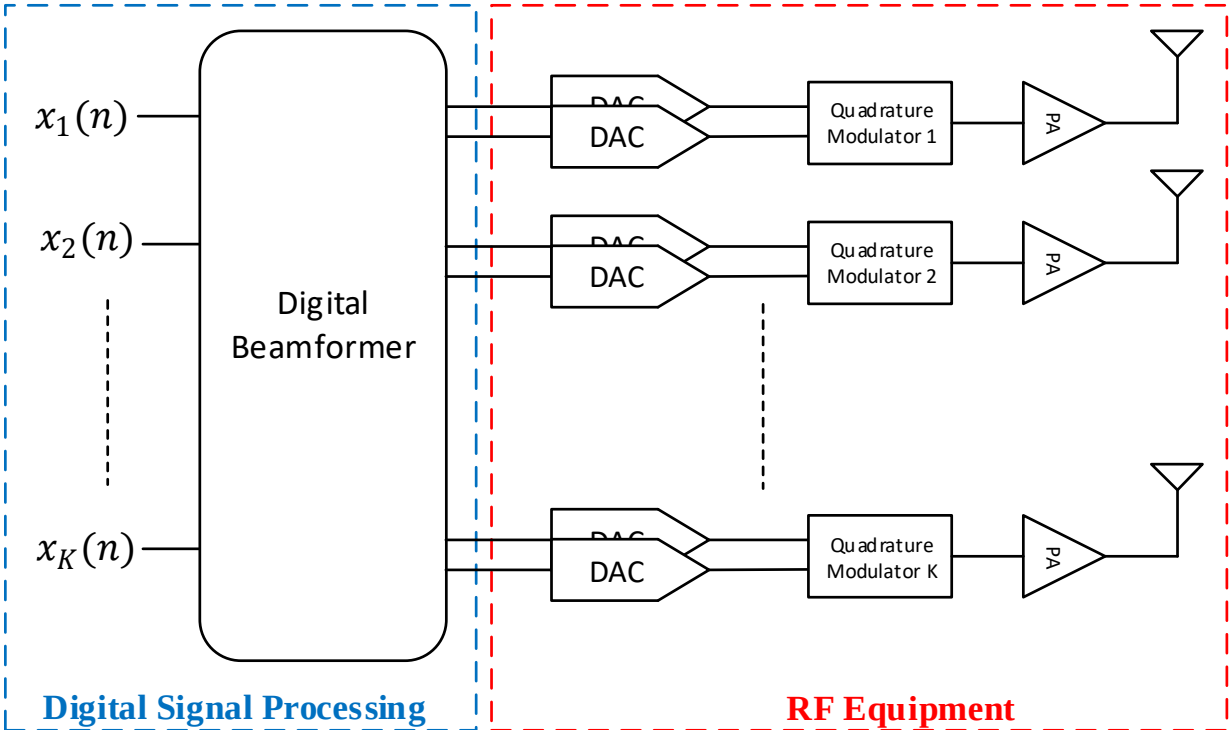

Figure 2.8: Digital Beamforming Architecture.

Digital Beamforming

Digital beamforming uses multiple transmitter chains in conjunction with one antenna per chain to create one or multiple concentrated electromagnetic beams that are used to transmit data. The digital beamforming architecture is shown in Fig. 2.8. Due to the fact that phase shifting and implementation of different beamforming algorithms are done in the digital domain, digital beamforming systems can be designed to be single or multi user. For example, in an 8 transmitter system, the first 4 and last 4 antennae can be used to bidirectionally transmit a stream of information to different receivers. As a trade-off to

these degrees of freedom, and the increased hardware complexity, digital beamforming is a costly, high power, high complexity method of implementing directional transmission of signals. [22]. Due to the high cost of implementing a large amount of transmitter chains, digital beamforming architectures are usually reserved for sub-6GHz applications [23].

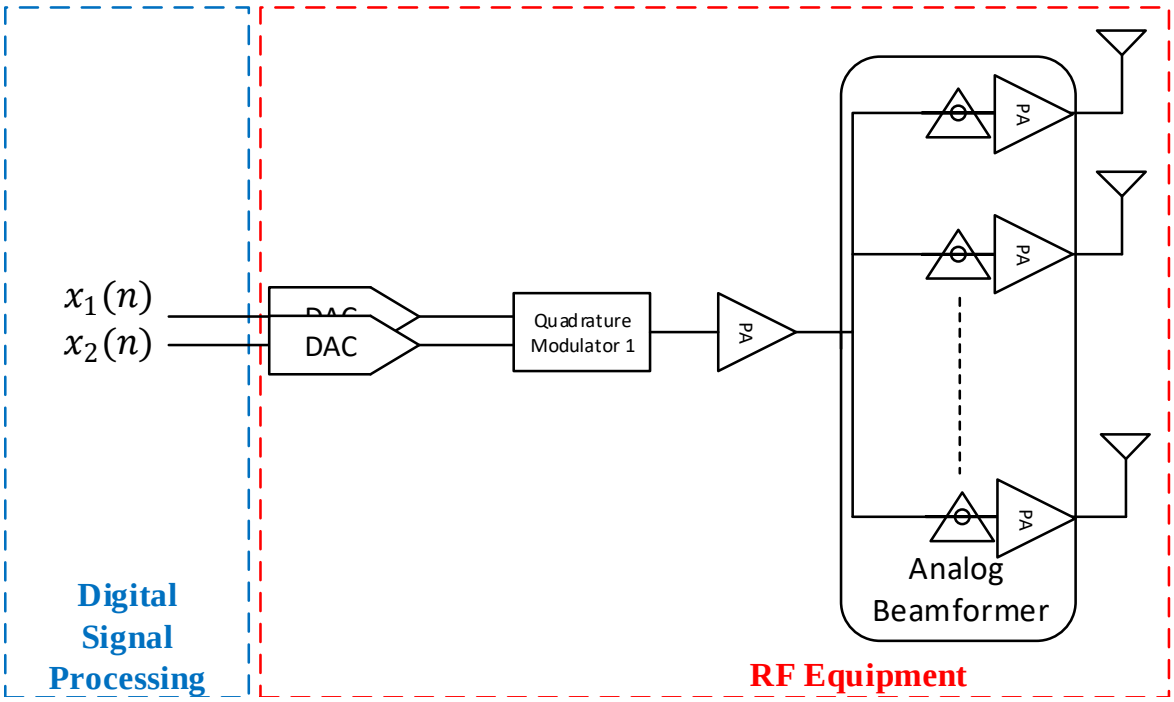

Figure 2.9: Analog Beamforming Architecture.

Analog Beamforming

Analog beamforming uses a single transmitter chain in conjunction with analog phase shifters which are connected to an antenna array to create a concentrated electromagnetic beam that is used to transmit data to a single user. The analog beamforming architecture is shown in Fig. 2.9. Analog beamforming systems are usually designed to serve one receiver. Analog beamforming is a cost effective, low power, low complexity method of implementing directional transmission of signals but suffers from lack of freedom in implementing different beamforming algorithms compared to digital and hybdrid beamforming [22].

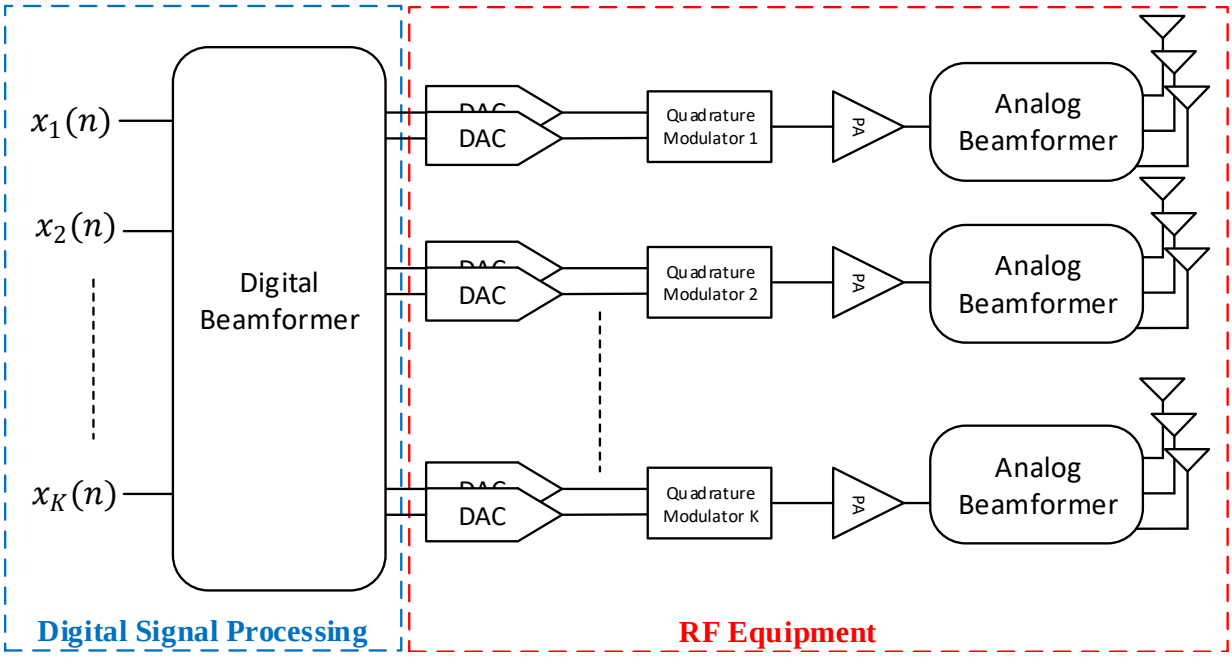

Figure 2.10: Hybrid Beamforming Architecture.

Hybrid Beamforming

Hybrid beamforming is a combination of digital beamforming and analog beamforming. It uses both individual transmitter chains as well as analog phase shifters, as shown in 2.10. This combination allows hybrid beamforming architectures to provide a compromise between the low complexity of analog beamforming and high degrees of freedom of digital beamforming. Therefore, hybrid beamforming architectures can have a large number of antennas and also implement complex beamforming algorithms. Since mmWave systems have higher path loss than sub-6GHz systems, large antenna gain, and therefore many antennae, is required due to the increase in path loss, therefore, hybrid beamforming is used in most mmWave beamforming designs [20], [24]. Once again, since this architecture has multiple transmitters, careful consideration should be taken in compensating for the compounding non-idealities of each transmitter chain.

2.2.3 Massive MIMO

In massive MIMO, a multi-antenna transmitter transfers multiple streams of data at the same frequency simultaneously to multiple receivers, as shown in Fig. 2.11. This is known as SMDA, such a system has an input output relationship described by .

$$\boldsymbol{y} = \boldsymbol{H}\boldsymbol{x}, \tag{2.4}$$

where

$$\boldsymbol{H} = \begin{bmatrix} h_{1,1} & h_{1,2} & \cdots & h_{1,M} \\ \vdots & \vdots & & \vdots \\ h_{K,1} & h_{K,2} & \cdots & h_{K,M} \end{bmatrix}.$$

The channel matrix, $\boldsymbol{H}$ can then be used to implement linear precoding techniques such maximum ratio transmission and zero-forcing [4]. There are also nonlinear signal processing techniques that offer higher capacity but are often difficult or highly computationally intensive to implement[25]. Massive MIMO architectures are usually considered to be sub 6GHz technologies [21].

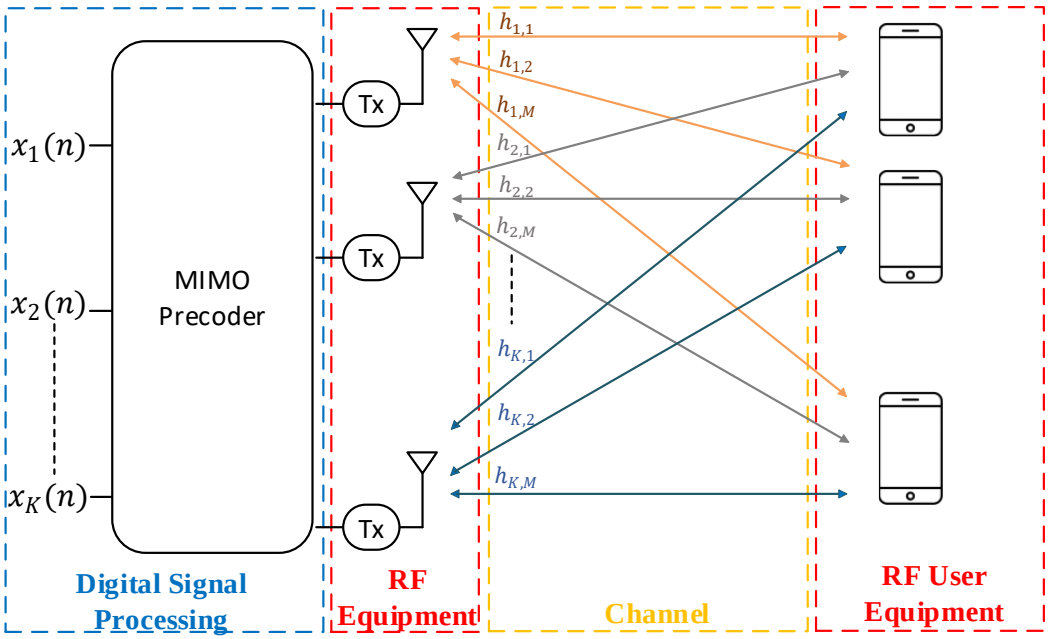

Figure 2.11: Massive MIMO System.

2.3 I/Q Imbalance in MIMO Systems

2.3.1 Overview of I/Q Imbalance in MIMO Systems

There are two aspects of I/Q Imbalance in MIMO systems that makes the task of tackling it different than I/Q Imbalance in SISO systems. First, the introduction of MIMO systems and other 5G technologies comes with the increase in bandwidth. This means that the I/Q imbalance identification and compensation scheme must be able to maintain accuracy over UWB in the GHz range. Secondly, in the case of SISO transmitter systems, one transmitter observation receiver (TOR) is needed to feedback the output signal to the baseband processing unit for I/Q imbalance identification.An example of a SISO system using a TOR is shown in Fig. 2.12.

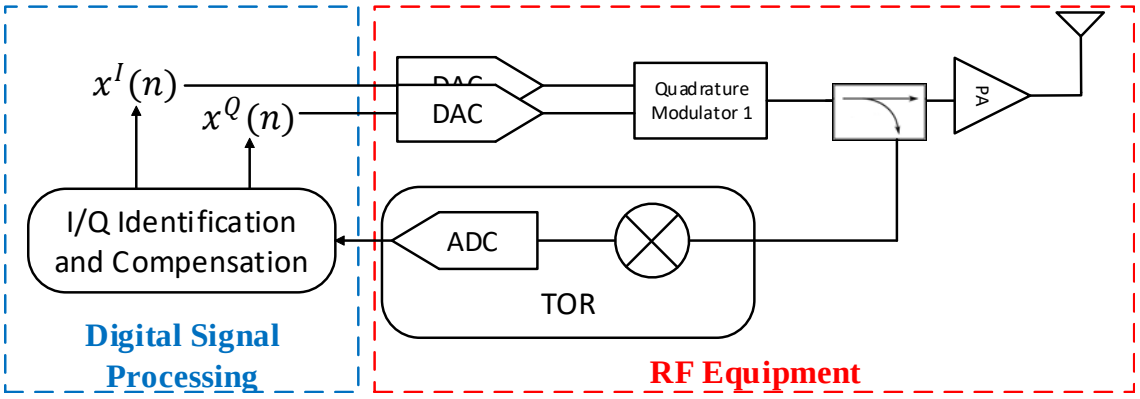

Figure 2.12: Single TOR single Tx

When extending this idea to the identification of I/Q imbalance and DPD in MIMO systems, there are two natural approaches. First, using multiple TORs, one for each RF chain as shown in Fig. 2.13. This approach suffers from a significant increase in hardware complexity, and this problem is compounded as 5G technologies fully develop and the number of transmitters increases. Another approach is using a single TOR augmented by a switch. The second approach has significantly lower hardware complexity compared to the first, but suffers from a lengthy identification process that may be unacceptable in real-time applications. Other works attempt to avoid the dilemma of designing a TOR by

simply lumping the I/Q compensation with the channel estimation done on the receiver side. Examples of both categories of work are shown in the literature review section.

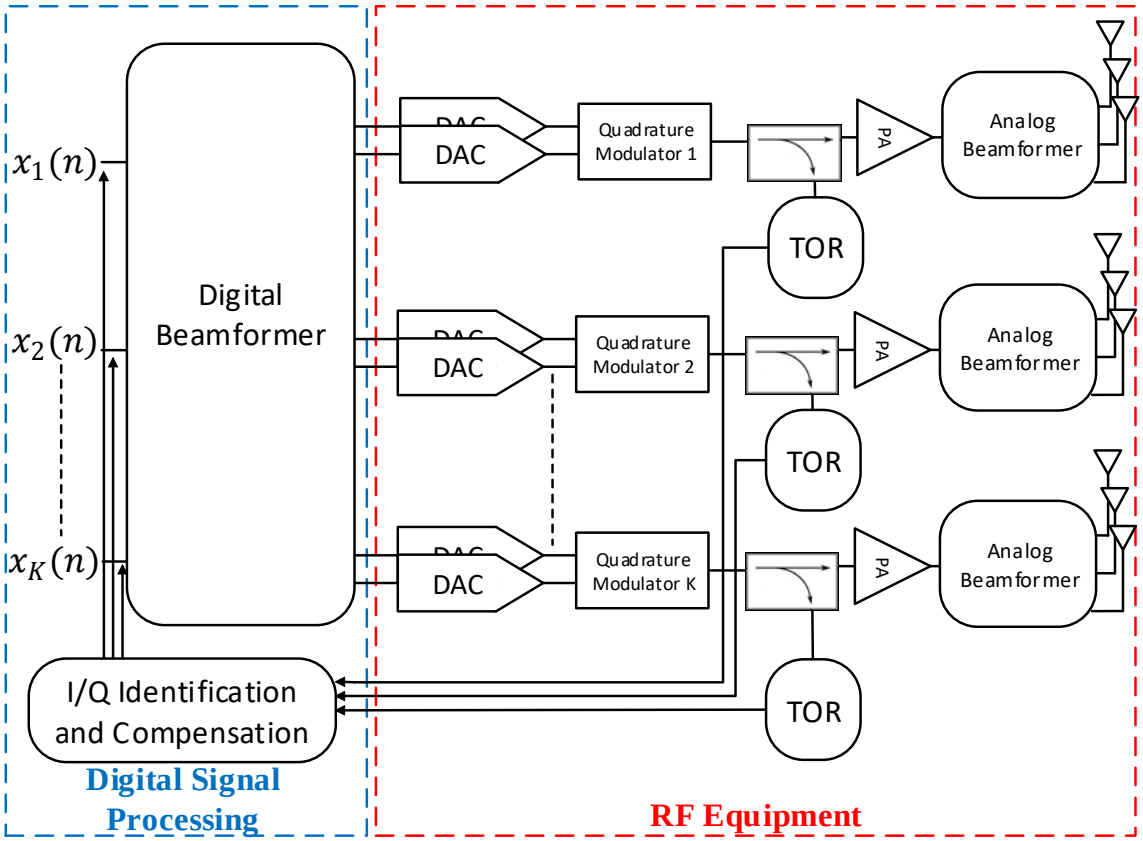

Figure 2.13: Multiple TOR

2.3.2 Literature Review

Transmitter Observation Receiver Based

Most approaches to solving the problem of I/Q imbalance in MIMO systems attempts to combine and compensate the problem of power amplifier (PA) non-linearity and I/Q imbalance into joint I/Q imbalance and DPD compensation. The authors in [26] use a composite neural network DPD model for joint mitigation of crosstalk, I/Q imbalance, and nonlin-

earity in MIMO Transmitters in their approach, they opt to use a single TOR augmented by a switch. This approach has significantly lower hardware complexity compared to multiple TORs, but suffers from a lengthy identification process that may be unacceptable in real-time applications.The authors in [27] present models for joint mitigation of static I/Q imbalance and MIMO PA distortion at the transmitter and use multiple TORs, thereby increasing hardware requirements. These compensation schemes suffer from a significant increase in computational complexity compared to independent I/Q compensation. This occurs because when the I/Q imbalance is not compensated before the non-linearity it significantly increases the linear memory order in the DPD [17] [18]. This increase leads to an exponential increase in the number of DPD coefficients needed to compensate the combined nonlinearity and I/Q imbalance.

No Transmitter Observation Receiver

To circumvent the I/Q imbalance identification and the underlying dilemma of choosing the number of TORs, in [28],[29],[30] the I/Q imbalance is lumped into the channel estimation process on the receiver side, thereby avoiding the use of any TOR. This approach significantly reduces the hardware complexity, however, it adds increases the computational burden on the receiver side. Moreover, the works in [28],[29],[30] have their limitations as they neglect the nonlinearity exhibited by PAs in the transmit chains. This is crucial because I/Q imbalance significantly affects the performance of the DPD [31] and moreover, if DPD is not preformed properly, the I/Q imbalance is heavily distorted by the nonlinearity exhibited by the PA, therefore it cannot be easily estimated on the receiver end.

Chapter 3

Compensation of Transmitter I/Q Imbalance in Millimeter-wave MIMO Systems

3.1 I/Q Imbalance Identification and Compensation Method for Transmitters in MIMO Systems

Fig. 3.1 shows the block diagram of a mmWave multi-user MIMO transmitter with a single TOR used to observe the combined output signal $y(t)$ of the K direct-conversion radio frequency (RF) chains. The combined output signal is used to identify and compensate for the inherent frequency-dependent I/Q imbalance in each chain. Accordingly, this leaves the challenge of separating the output signals' envelopes from $y_k^{RF}(t)$, for each modulator, from the combined output signal, $y(t)$, in order to concurrently identify the corresponding I/Q imbalance. In this thesis, we first present the model of the single chain in Fig. 3.1 [10]. Using this model we develop a method of identifying the I/Q imbalances for multiple transmitter chains. Finally, the I/Q imbalances are compensated for by calculating appropriate compensators which offset the I/Q imbalance inherent in quadrature modulators.

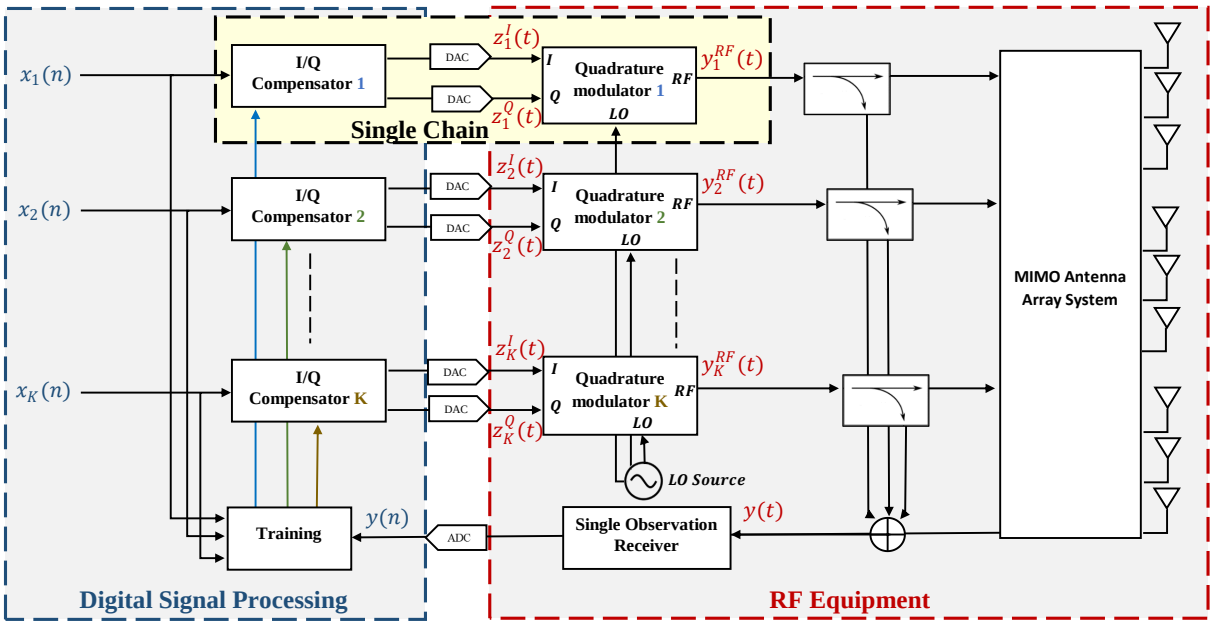

Figure 3.1: Block diagram for a mmWave MIMO transmitter system with K independent transmit chains utilizing a single TOR for compensation.

3.1.1 I/Q Compensator and Quadrature Modulator Model

To formulate the I/Q imbalance compensation for MIMO systems, the model first proposed in [10] and adopted in [11] and [13], for a single chain transmitter (Tx) is adopted. The discrete baseband model of the single chain highlighted in Fig. 3.1 is shown in Fig. 3.2. The quadrature modulator is modeled in discrete baseband by four real-valued finite impulse response (FIR) filters, $\boldsymbol{h}_k^{11}$, $\boldsymbol{h}_k^{21}$, $\boldsymbol{h}_k^{12}$, and $\boldsymbol{h}_k^{22}$, as shown in Fig. 3.2(b). The filters that constitute the quadrature modulator are known as I/Q Imbalance filters. In the ideal case of no I/Q imbalance $\boldsymbol{h}_k^{21}$ and $\boldsymbol{h}_k^{12}$ would be equal to zero while $\boldsymbol{h}_k^{11}$ and $\boldsymbol{h}_k^{22}$ would be single-tap FIR filters of zero phase and magnitude one. The I/Q compensator designed to achieve the ideal quadrature modulator behavior consists of four real-valued FIR filters, $\boldsymbol{g}_k^{11}$, $\boldsymbol{g}_k^{21}$, $\boldsymbol{g}_k^{12}$, and $\boldsymbol{g}_k^{22}$, as shown in Fig. 3.2(a). In the sections below we first outline how to estimate the I/Q imbalance filters in Fig. 3.2(b). Next, from those estimates we design the compensation filters in Fig. 3.2(a) which will be applied to the original input signal

thereby cancelling the effect of the I/Q imbalance.

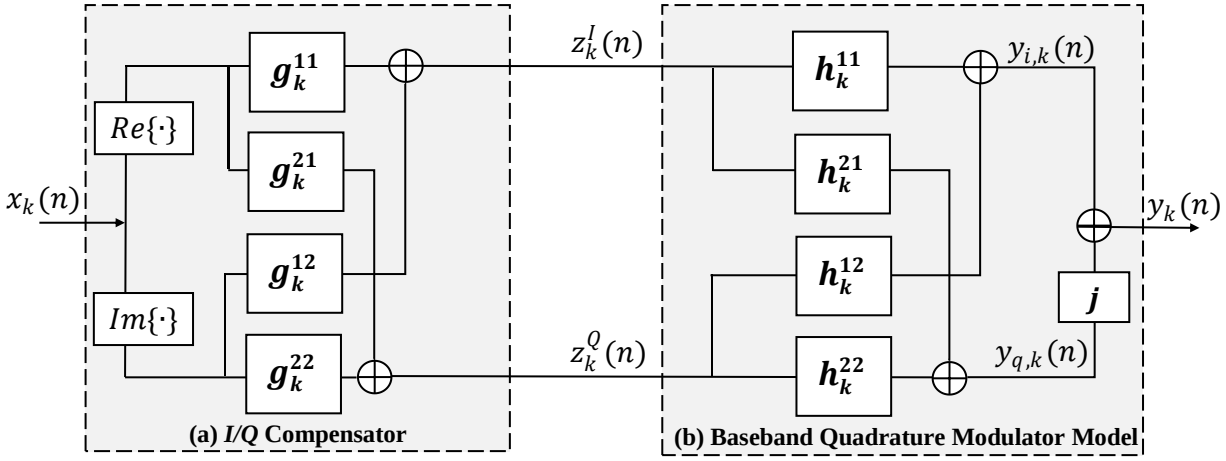

Figure 3.2: (a) Block diagram of the I/Q compensator. (b) Block diagram of the baseband model of a quadrature modulator for a single transmitter chain.

3.1.2 I/Q Imbalance Identification

For the k^{th} quadrature modulator, the output $y_k(n)$, which is the discrete complex baseband version of $y_k^{RF}(t)$ in Fig. 3.1, is related to the discrete baseband in-phase $z_k^I(n)$ and quadrature $z_k^Q(n)$ inputs to the quadrature modulator by

$$y_k(n) = z_k^I(n) * h_k^I(n) + z_k^Q(n) * h_k^Q(n), \tag{3.1}$$

where

$$h_k^I(n) = h_k^{11}(n) + jh_k^{21}(n) \tag{3.2}$$

$$h_k^Q(n) = h_k^{12}(n) + jh_k^{22}(n) \tag{3.3}$$

are the equivalent complex-valued I/Q imbalance filters. In order to compensate for the I/Q imbalance, we must first estimate $\boldsymbol{h}_k^I$ and $\boldsymbol{h}_k^Q$. To accomplish this, we first express 3.1 in vector form as

$$\boldsymbol{y}_k = \boldsymbol{Z}_k^I \boldsymbol{h}_k^I + \boldsymbol{Z}_k^Q \boldsymbol{h}_k^Q, \tag{3.4}$$

where

$$\boldsymbol{y}_k = [y_k(L-1), \cdots, y_k(N-1)]^T$$
$$\boldsymbol{h}_k^I = [h_k^I(0), \cdots, h_k^I(L-1)]^T$$
$$\boldsymbol{h}_k^Q = [h_k^Q(0), \cdots, h_k^Q(L-1)]^T$$
$$\boldsymbol{Z}_k^I = Re\{\boldsymbol{Z}_k\}$$
$$\boldsymbol{Z}_k^Q = Im\{\boldsymbol{Z}_k\}$$

and

$$\boldsymbol{Z}_k = \begin{bmatrix} z_k(L-1) & z_k(L-2) & \cdots & z_k(0) \\ z_k(L) & z_k(L-1) & \cdots & z_k(1) \\ \vdots & \vdots & & \vdots \\ z_k(N-1) & z_k(N-2) & \cdots & z_k(N-L) \end{bmatrix}.$$

In the above, L designates the length of the I/Q imbalance filters and N denotes the number samples of the input signal $z_k(n)$. As shown in Fig. 3.1, the use of a single TOR captures the vector-summed outputs of all the quadrature modulators, i.e.,

$$\boldsymbol{y} = \sum_{k=1}^{K} \boldsymbol{y}_k. \tag{3.5}$$

Combining (3.3) and (3.5) we arrive at

$$\boldsymbol{y} = \sum_{k=1}^{K} \boldsymbol{Z}_k^I \boldsymbol{h}_k^I + \boldsymbol{Z}_k^Q \boldsymbol{h}_k^Q. \tag{3.6}$$

To identify the I/Q imbalance filters we use a least-squares estimate approach and define the cost function as

$$J = \left\| \boldsymbol{y} - \sum_{k=1}^{K} (\boldsymbol{Z}_k^I \boldsymbol{h}_k^I + \boldsymbol{Z}_k^Q \boldsymbol{h}_k^Q) \right\|^2. \tag{3.7}$$

The minimum value of 3.7 is found by taking the partial derivative of 3.7 with respect to each $\hat{\boldsymbol{h}}_k^I$ and $\hat{\boldsymbol{h}}_k^Q$ and equating the results to zero [32]. This yields the least-squares estimate of the I/Q imbalance filters expressed below

$$\hat{\boldsymbol{h}} = (\boldsymbol{Q}^T \boldsymbol{Q})^{-1} \boldsymbol{Q}^T \boldsymbol{y}, \tag{3.8}$$

where

$$\boldsymbol{Q} = \begin{bmatrix} \boldsymbol{Z}_1^I & \boldsymbol{Z}_1^Q & \cdots & \boldsymbol{Z}_K^I & \boldsymbol{Z}_K^Q \end{bmatrix}$$

$$\hat{\boldsymbol{h}} = \begin{bmatrix} \hat{\boldsymbol{h}}_1^I \\ \hat{\boldsymbol{h}}_1^Q \\ \vdots \\ \hat{\boldsymbol{h}}_K^I \\ \hat{\boldsymbol{h}}_K^Q \end{bmatrix}.$$

3.1.3 I/Q Compensator Filter Calculation

With the I/Q imbalance filters $\hat{\boldsymbol{h}}_k^{11}$, $\hat{\boldsymbol{h}}_k^{21}$, $\hat{\boldsymbol{h}}_k^{12}$ and $\hat{\boldsymbol{h}}_k^{22}$ estimated, from 3.8 the corresponding I/Q compensation filters $\boldsymbol{g}_k^{11}$, $\boldsymbol{g}_k^{21}$, $\boldsymbol{g}_k^{12}$ and $\boldsymbol{g}_k^{22}$ must satisfy the z-domain expression below (see [11] and Fig. 3.2):

$$\begin{bmatrix} \hat{\boldsymbol{H}}_k^{11}(z) & \hat{\boldsymbol{H}}_k^{12}(z) \\ \hat{\boldsymbol{H}}_k^{21}(z) & \hat{\boldsymbol{H}}_k^{22}(z) \end{bmatrix} \begin{bmatrix} \boldsymbol{G}_k^{11}(z) & \boldsymbol{G}_k^{12}(z) \\ \boldsymbol{G}_k^{21}(z) & \boldsymbol{G}_k^{22}(z) \end{bmatrix} = I_{2\times 2}. \tag{3.9}$$

Multiplying both sides of 3.9 by the matrix,

$$\begin{bmatrix} \hat{\boldsymbol{H}}_k^{22}(z) & -\hat{\boldsymbol{H}}_k^{12}(z) \\ -\hat{\boldsymbol{H}}_k^{21}(z) & \hat{\boldsymbol{H}}_k^{11}(z) \end{bmatrix},$$

and applying the inverse z-transform, we obtain

$$h_k^D(n) * g_k^{11}(n) = \hat{h}_k^{22}(n) \tag{3.10}$$

$$h_k^D(n) * g_k^{12}(n) = -\hat{h}_k^{12}(n) \tag{3.11}$$

$$h_k^D(n) * g_k^{21}(n) = -\hat{h}_k^{21}(n) \tag{3.12}$$

$$h_k^D(n) * g_k^{22}(n) = \hat{h}_k^{11}(n) \tag{3.13}$$

where $h_k^D(n)$ is the determinant:

$$\boldsymbol{h}_k^D(n) = \hat{\boldsymbol{h}}_k^{11}(n) * \hat{\boldsymbol{h}}_k^{22}(n) - \hat{\boldsymbol{h}}_k^{12}(n) * \hat{\boldsymbol{h}}_k^{21}.(n) \tag{3.14}$$

Rewriting (3.10) - (3.14) in matrix form,

$$\boldsymbol{h}_k^{22} = \boldsymbol{H}_k^D \hat{\boldsymbol{g}}_k^{11} \tag{3.15}$$

$$\boldsymbol{h}_k^{12} = -\boldsymbol{H}_k^D \hat{\boldsymbol{g}}_k^{12} \tag{3.16}$$

$$\boldsymbol{h}_k^{21} = -\boldsymbol{H}_k^D \hat{\boldsymbol{g}}_k^{21} \tag{3.17}$$

$$\boldsymbol{h}_k^{11} = \boldsymbol{H}_k^D \hat{\boldsymbol{g}}_k^{22}, \tag{3.18}$$

where

$$\hat{\boldsymbol{h}}_k^{ij} = [\hat{\boldsymbol{h}}_k^{ij}(0), \cdots, \hat{\boldsymbol{h}}_k^{ij}(L-1)]^T$$
$$\boldsymbol{g}_k^{ij} = [\boldsymbol{g}_k^{ij}(0), \cdots, \boldsymbol{g}_k^{ij}(M-1)]^T,$$

for $i, j \epsilon \{1, 2\}$. In the above, L designates the length of the I/Q imbalance filters and $\boldsymbol{H}_k^D$ is defined as the convolution matrix of $h_k^D(n)$. The I/Q compensation filters, $\boldsymbol{g}_k^{ij}$, that solve 3.15 - 3.18 may be very long or have infinite impulse response (IIR) and are thus limited to an appropriate length M that approximates the IIR solution. To identify the I/Q compensation filters we use a least-squares estimate approach. The least-squares estimates, $\hat{\boldsymbol{g}}_k^{11}$, $\hat{\boldsymbol{g}}_k^{21}$, $\hat{\boldsymbol{g}}_k^{12}$ and $\hat{\boldsymbol{g}}_k^{22}$, of the I/Q compensation filter for each transmitter are then found to be,

$$\hat{\boldsymbol{g}}_k^{11} = (\boldsymbol{H}_k^{D^T} \boldsymbol{H}_k^D)^{-1} \boldsymbol{H}_k^{D^T} \hat{\boldsymbol{h}}_k^{22} \tag{3.19}$$

$$\hat{\boldsymbol{g}}_k^{12} = -(\boldsymbol{H}_k^{D^T} \boldsymbol{H}_k^D)^{-1} \boldsymbol{H}_k^{D^T} \hat{\boldsymbol{h}}_k^{12} \tag{3.20}$$

$$\hat{\boldsymbol{g}}_k^{21} = -(\boldsymbol{H}_k^{D^T} \boldsymbol{H}_k^D)^{-1} \boldsymbol{H}_k^{D^T} \hat{\boldsymbol{h}}_k^{21} \tag{3.21}$$

$$\hat{\boldsymbol{g}}_k^{22} = (\boldsymbol{H}_k^{D^T} \boldsymbol{H}_k^D)^{-1} \boldsymbol{H}_k^{D^T} \hat{\boldsymbol{h}}_k^{11}. \tag{3.22}$$

The compensation filters can now be applied before transmission as follows

$$z_k^I(n) = x_k^I(n) * \hat{g}_k^{11}(n) + x_k^Q(n) * \hat{g}_k^{12}(n) \tag{3.23}$$

$$z_k^Q(n) = x_k^Q(n) * \hat{g}_k^{22}(n) + x_k^I(n) * \hat{g}_k^{21}(n). \tag{3.24}$$

3.2 Choice of Training Signal

In practical RF chains, the PA exhibits non-negligible non-linearity that would compromise the EVM and ACPR of the transmitted signal. Without compensation for this non-linearity, the occupied bandwidth at the output of such a PA is expanded compared to the bandwidth of the original signal at the input. An expansion factor of 5x is common, i.e., a 100 MHz modulation bandwidth at the input of the RF chain would result in a 500 MHz modulation bandwidth at the PA output. To compensate for the non-linearity of the PA, baseband DPD [17] is commonly applied before I/Q modulation to compensate for the passband non-linearity of the PA. This DPD is also a nonlinear operation, and thus the modulation bandwidth at the output of the predistorter is typically 5x that of the original RF signal and the DPD operates at 5x the Nyquist sampling rate of the original signal. Nevertheless, as the DPD and PA nonlinearities cancel each other, resulting in linear operation overall, the modulation bandwidth at the PA output after linearization is then that of the original signal. This nonlinearity cancellation is critically dependent on the accuracy of the quadrature modulation operation over the predistorted signal bandwidth [31]. Therefore, the I/Q imbalance identification and compensation must maintain acceptable accuracy over the entire bandwidth of the predistorted signal. i.e., the I/Q imbalance correction for an original modulated signal of 800 MHz should extend over a bandwidth of 4 GHz.

In [11] compensation for out-of-band I/Q imbalance is not performed since it is assumed a well-designed quadrature modulator would achieve an image-rejection ratio of 40 dB, therefore leaving the image caused by I/Q imbalance in the out-of-band region below the noise floor of the receiver. However, for many commercially available quadrature modulators, this is not the case. By contrast, in [12] and [33], the I/Q imbalance calibration was conducted using a training signal with a flat Power Spectral Density (PSD) over the targeted predistortion bandwidth. Although this conventional approach provides significant performance increase when compared to no I/Q compensation, it fails to take into account the specific spectral shape of the predistorted signals that arise from the use cases of DPD for PAs. Predistorted signals have most of their power concentrated within the original signal bandwidth (called the in-band) with spectral regrowth (of lower power

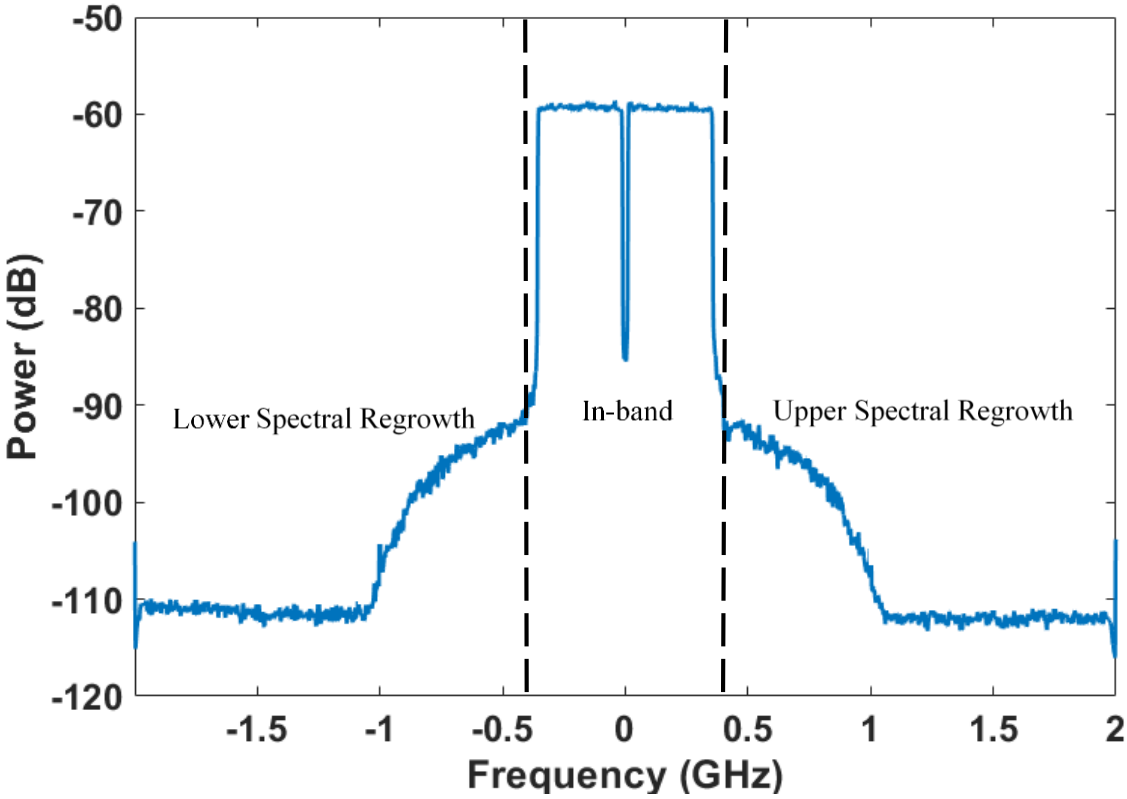

Figure 3.3: Typical PSD of a predistorted signal at the input of a PA.

spectral density) in adjacent bands. An example of such a pre-distorted signal can be seen in Fig. 3.3.

Therefore, a judiciously designed signal with a PSD that achieves optimal compensation performance is beneficial. In the upcoming subsection, the training signal PSD that minimizes the mean squared error (MSE) between i) the actual output of the physical quadrature modulator and ii) the predicted output based on the estimated I/Q imbalance filters, is found. Specifically, in the upcoming subsection, it is shown that for optimal compensation the training signal should be chosen such that its PSD is the same as the PSD at the output of the predistorter, such as the one shown in Fig. 3.3. It is of note that this MSE evaluates the accuracy of the filter coefficients in predicting the systems true output

over the entire linearization bandwidth.

Finding the Ideal Training Signal

Consider a noiseless I/Q modulator system that has an input-output relation characterized by,

$$y(n) = z^I(n) * h^I(n) + z^Q(n) * h^Q(n),$$

In the above, $z^I(n)$ and $z^Q(n)$ are the real and imaginary components of the input signal and the $h^I(n)$ and $h^Q(n)$ are FIR filters each containing K unknown complex taps. This can be represented in vector form as,

$$[y(N), y(N-1), \cdots, y(K)]^T \triangleq \boldsymbol{y} = \boldsymbol{Q}\boldsymbol{h} \tag{3.25}$$

where

$$\boldsymbol{Q} = [\boldsymbol{Z}^I \ \boldsymbol{Z}^Q]$$

$$\boldsymbol{h} = \begin{bmatrix} \boldsymbol{h}^I \\ \boldsymbol{h}^Q \end{bmatrix}$$

$$\boldsymbol{h}^I = [h^I(0), \cdots, h^I(K-1)]^T$$

$$\boldsymbol{h}^Q = [h^Q(0), \cdots, h^Q(K-1)]^T$$

$$\boldsymbol{Z}^I = Re\{\boldsymbol{Z}\}$$

$$\boldsymbol{Z}^Q = Im\{\boldsymbol{Z}\}$$

$$\boldsymbol{Z} = \begin{bmatrix} z(N) & z(N-1) & \cdots & z(N-K+1) \\ z(N-1) & z(N-2) & \cdots & z(N-K) \\ \vdots & \vdots & & \vdots \\ z(K) & z(K-1) & \cdots & z(1) \end{bmatrix}.$$

To estimate the coefficients in this system we use a training stage. Since K is usually large for physical systems, we wish to estimate this system using only $2L < 2K$ coefficients specified by the vector

$$\hat{\boldsymbol{h}} = \begin{bmatrix} \hat{\boldsymbol{h}}^I \\ \hat{\boldsymbol{h}}^Q \end{bmatrix}, \tag{3.26}$$

where

$$\hat{\boldsymbol{h}}^I = [\hat{h}^I(0), \cdots, \hat{h}^I(L-1)]^T$$
$$\hat{\boldsymbol{h}}^Q = [\hat{h}^Q(0), \cdots, \hat{h}^Q(L-1)]^T.$$

The goal is to determine the training signal to be used in the estimation of $\hat{h}$ that minimizes the MSE between the actual output of the system generated by the physical quadrature modulator during the verification stage, $\boldsymbol{y}_{ve} = [y_{ve}(N), y_{ve}(N-1), \cdots, y_{ve}(K)]^T$ and our prediction of the output based on the calculated I/Q imbalance filters, $\hat{\boldsymbol{y}}_{ve} = [\hat{y}_{ve}(N), \hat{y}_{ve}(N-1), \cdots, \hat{y}_{ve}(K)]^T$, i.e., to minimize

$$J = \left\| \boldsymbol{y}_{ve} - \hat{\boldsymbol{y}}_{ve} \right\|^2, \tag{3.27}$$

where

$$\boldsymbol{y}_{ve} = \boldsymbol{Q}_{ve}\boldsymbol{h} \tag{3.28}$$
$$\hat{\boldsymbol{y}}_{ve} = \bar{\boldsymbol{Q}}_{ve}\hat{\boldsymbol{h}} \tag{3.29}$$

and

$$\boldsymbol{Q}_{ve} = [\boldsymbol{Z}^I_{ve}\ \boldsymbol{Z}^Q_{ve}]$$
$$\bar{\boldsymbol{Q}}_{ve} = [\bar{\boldsymbol{Z}}^I_{ve}\ \bar{\boldsymbol{Z}}^Q_{ve}]$$
$$\boldsymbol{Z}^I_{ve} = Re\{\boldsymbol{Z_{ve}}\}$$
$$\boldsymbol{Z}^Q_{ve} = Im\{\boldsymbol{Z_{ve}}\}$$
$$\bar{\boldsymbol{Z}}^I_{ve} = Re\{\bar{\boldsymbol{Z}}_{\boldsymbol{ve}}\}$$
$$\bar{\boldsymbol{Z}}^Q_{ve} = Im\{\bar{\boldsymbol{Z}}_{\boldsymbol{ve}}\}$$

$$\boldsymbol{Z}_{ve} = \begin{bmatrix} z_{ve}(N) & z_{ve}(N-1) & \cdots & z_{ve}(N-K+1) \\ z_{ve}(N-1) & z_{ve}(N-2) & \cdots & z_{ve}(N-K) \\ \vdots & \vdots & & \vdots \\ z_{ve}(K) & z_{ve}(K-1) & \cdots & z_{ve}(1) \end{bmatrix}$$

$$\bar{\boldsymbol{Z}}_{ve} = \begin{bmatrix} z_{ve}(N) & z_{ve}(N-1) & \cdots & z_{ve}(N-L+1) \\ z_{ve}(N-1) & z_{ve}(N-2) & \cdots & z_{ve}(N-L) \\ \vdots & \vdots & & \vdots \\ z_{ve}(K) & z_{ve}(K-1) & \cdots & z_{ve}(K-L+1) \end{bmatrix},$$

where $Re\{z_{ve}(n)\}$ and $Im\{z_{ve}(n)\}$ are the real and imaginary components of a zero-mean wide-sense stationary ergodic verification signal that is used to verify the efficacy of our estimation of $\hat{\boldsymbol{h}}$. Substituting 3.28 and 3.29 into 3.27 we arrive at the cost function,

$$J = \left\| \boldsymbol{Q}_{ve}\boldsymbol{h} - \bar{\boldsymbol{Q}}_{ve}\hat{\boldsymbol{h}} \right\|^2, \tag{3.30}$$

We now show that 3.30 can be minimized if the estimate h ÌĆ is calculated during the training phase using a training signal, $z_{tr}(n)$, that has the same second order statistics, or equivalently the same PSD, as the verification signal $z_{ve}(n)$. We do this by representing 3.30 in terms of the second order statistics of both the training and verification signals, then deriving the minimum solution. We begin by first identifying the estimate $\hat{h}$ in terms of the second order statistics of the training signal $z_{tr}(n)$. To estimate $\hat{h}$ we use a training stage characterized by the input-output relationship,

$$[y_{tr}(N), y_{tr}(N-1), \cdots, y_{tr}(K)]^T \triangleq \boldsymbol{y}_{tr} = \boldsymbol{Q}_{tr}\boldsymbol{h} \tag{3.31}$$

where

$$\boldsymbol{Q} = [\boldsymbol{Z}_{tr}^I \ \boldsymbol{Z}_{tr}^Q]$$

$$\boldsymbol{Z}_{tr}^I = Re\{\boldsymbol{Z}_{tr}\}$$

$$\boldsymbol{Z}_{tr}^Q = Im\{\boldsymbol{Z}_{tr}\}$$

$$\boldsymbol{Z}_{tr} = \begin{bmatrix} z_{tr}(N) & z_{tr}(N-1) & \cdots & z_{tr}(N-K+1) \\ z_{tr}(N-1) & z_{tr}(N-2) & \cdots & z_{tr}(N-K) \\ \vdots & \vdots & & \vdots \\ z_{tr}(K) & z_{tr}(K-1) & \cdots & z_{tr}(1) \end{bmatrix}.$$

and $Re\{z_{tr}(n)\}$ and $Im\{z_{tr}(n)\}$ are the real and imaginary components of the zero-mean wide-sense stationary ergodic training signal that is used to estimate $\hat{\boldsymbol{h}}$. Since the system is to be identified using $2L < 2K$ coefficents, the least-squares estimate of these coefficients from $\boldsymbol{y}_{tr}$ is,

$$\hat{\boldsymbol{h}} = (\bar{\boldsymbol{Q}}_{tr}^T\bar{\boldsymbol{Q}}_{tr})^{-1}\bar{\boldsymbol{Q}}_{tr}^T\boldsymbol{y}_{tr} \tag{3.32}$$

where

$$\bar{\boldsymbol{Q}}_{tr} = [\bar{\boldsymbol{Z}}_{tr}^I \ \bar{\boldsymbol{Z}}_{tr}^Q]$$

$$\bar{\boldsymbol{Z}}_{tr}^{I} = Re\{\bar{\boldsymbol{Z}}_{tr}\}$$
$$\bar{\boldsymbol{Z}}_{tr}^{Q} = Im\{\bar{\boldsymbol{Z}}_{tr}\}$$
$$\bar{\boldsymbol{Z}}_{tr} = \begin{bmatrix} z_{tr}(N) & z_{tr}(N-1) & \cdots & z_{tr}(N-L+1) \\ z_{tr}(N-1) & z_{tr}(N-2) & \cdots & z_{tr}(N-L) \\ \vdots & \vdots & & \vdots \\ z_{tr}(K) & z_{tr}(K-1) & \cdots & z_{tr}(K-L+1) \end{bmatrix}.$$

Substituting 3.31 into 3.32 we arrive at

$$\hat{\boldsymbol{h}} = (\bar{\boldsymbol{Q}}_{tr}^{T}\bar{\boldsymbol{Q}}_{tr})^{-1}\bar{\boldsymbol{Q}}_{tr}^{T}\boldsymbol{Q}_{tr}\boldsymbol{h} \tag{3.33}$$

For very large N, the second order statistics of an autocorrelation ergodic WSS signal converge to the ensemble ones. This means that, for very large N, we can represent the estimate $\hat{\boldsymbol{h}}$ in terms of the second order statistics of the real and imaginary part of the training signal. Let,

$$r_{tr}^{ab}(u,N) = \frac{1}{N}\sum_{n=0}^{N-u} z_{tr}^{a}(n)z_{tr}^{b}(n+u).$$

where a, bÏt$\{I,Q\}$.Then as $N \to \infty$,

$$r_{tr}^{ab}(u,N) \to E\{r_{tr}^{a}(n)r_{tr}^{b}(n+u)\} = r_{tr}^{ab}(u),$$

where, convergence is in the MSE sense, and $r_{tr}^{ab}(u)$ is the cross-correlation function of $z_t r^a(n)$ and $z_t r^b(n)$.Therefore, 3.33 converges to

$$\hat{\boldsymbol{h}} = \bar{\boldsymbol{R}}_{tr}^{-1}\hat{\boldsymbol{R}}_{tr}\boldsymbol{h}, \tag{3.34}$$

where

$$\bar{\boldsymbol{R}}_{tr} = \begin{bmatrix} \bar{\boldsymbol{R}}_{tr}^{II} & \bar{\boldsymbol{R}}_{tr}^{IQ} \\ \bar{\boldsymbol{R}}_{tr}^{QI} & \bar{\boldsymbol{R}}_{tr}^{QQ} \end{bmatrix}$$
$$\hat{\boldsymbol{R}}_{tr} = \begin{bmatrix} \hat{\boldsymbol{R}}_{tr}^{II} & \hat{\boldsymbol{R}}_{tr}^{IQ} \\ \hat{\boldsymbol{R}}_{tr}^{QI} & \hat{\boldsymbol{R}}_{tr}^{QQ} \end{bmatrix}$$
$$\bar{\boldsymbol{R}}_{tr}^{ab} = \begin{bmatrix} r_{tr}^{ab}(0) & r_{tr}^{ab}(1) & \cdots & r_{tr}^{ab}(L-1) \\ r_{tr}^{ab}(1) & r_{tr}^{ab}(0) & \cdots & r_{tr}^{ab}(L-2) \\ \vdots & \vdots & & \vdots \\ r_{tr}^{ab}(L-1) & r_{tr}^{ab}(L-2) & \cdots & r_{tr}^{ab}(0) \end{bmatrix}.$$

$$\hat{\boldsymbol{R}}_{tr}^{ab} = \begin{bmatrix} & r_{tr}^{ab}(L) & r_{tr}^{ab}(L-1) & \cdots & r_{tr}^{ab}(K-1) \\ \bar{\boldsymbol{R}}_{tr}^{ab} & r_{tr}^{ab}(L-1) & r_{tr}^{ab}(L-2) & \cdots & r_{tr}^{ab}(K-2) \\ & \vdots & \vdots & & \vdots \\ & r_{tr}^{ab}(1) & r_{tr}^{ab}(2) & \cdots & r_{tr}^{ab}(K-L) \end{bmatrix}.$$

and a, bÏţ$\{I, Q\}$.$\bar{\boldsymbol{R}}_{tr}$ and $\hat{\boldsymbol{R}}_{tr}$ represent the joint second-order statistics of $z_{tr}^{I}(n)$ and $z_{tr}^{Q}(n)$. Letting,

$$\boldsymbol{B} = \bar{\boldsymbol{R}}_{tr}^{-1}\bar{\boldsymbol{R}}_{tr} \tag{3.35}$$

we arrive at

$$\hat{\boldsymbol{h}} = \boldsymbol{B}\boldsymbol{h} \tag{3.36}$$

Expanding the cost function in 3.30 and substituting 3.36 we arrive at 3.37,

$$\begin{aligned} J &= (\boldsymbol{Q}_{ve}\boldsymbol{h} - \bar{\boldsymbol{Q}}_{ve}\hat{\boldsymbol{h}})^H(\boldsymbol{Q}_{ve}\boldsymbol{h} - \bar{\boldsymbol{Q}}_{ve}\hat{\boldsymbol{h}}) \\ &= \boldsymbol{h}^H\boldsymbol{Q}_{ve}^T\boldsymbol{Q}_{ve}\boldsymbol{h} - 2\hat{\boldsymbol{h}}^H\bar{\boldsymbol{Q}}_{ve}^T\boldsymbol{Q}_{ve}\boldsymbol{h} + \hat{\boldsymbol{h}}^H\bar{\boldsymbol{Q}}_{ve}^T\bar{\boldsymbol{Q}}_{ve}\hat{\boldsymbol{h}} \\ &= \boldsymbol{h}^H\boldsymbol{Q}_{ve}^T\boldsymbol{Q}_{ve}\boldsymbol{h} - 2\boldsymbol{h}^H\boldsymbol{B}^T\bar{\boldsymbol{Q}}_{ve}^T\boldsymbol{Q}_{ve}\boldsymbol{h} + \boldsymbol{h}^H\boldsymbol{B}^T\bar{\boldsymbol{Q}}_{ve}^T\bar{\boldsymbol{Q}}_{ve}\boldsymbol{B}\boldsymbol{h} \end{aligned} \tag{3.37}$$

Once again, for very large N, we can express the cost function in terms of the joint second-order statistics of the verification signal, $z_{ve}^{I}(n)$ and $z_{ve}^{Q}(n)$.Let,

$$r_{ve}^{ab}(u) = E\{r_{ve}^{a}(n)r_{ve}^{b}(n+u)\},$$

and a, bÏţ$\{I, Q\}$.Then for very large N, the cost function in 3.37 converges to

$$J = \boldsymbol{h}^H\boldsymbol{R}_{ve}\boldsymbol{h} - 2\boldsymbol{h}^H\boldsymbol{B}^T\hat{\boldsymbol{R}}_{ve}\boldsymbol{h} + \boldsymbol{h}^H\boldsymbol{B}^T\bar{\boldsymbol{R}}_{ve}\boldsymbol{B}\boldsymbol{h} \tag{3.38}$$

where

$$\boldsymbol{R}_{ve} = \begin{bmatrix} \boldsymbol{R}_{ve}^{II} & \boldsymbol{R}_{ve}^{IQ} \\ \boldsymbol{R}_{ve}^{QI} & \boldsymbol{R}_{ve}^{QQ} \end{bmatrix}$$

$$\bar{\boldsymbol{R}}_{ve} = \begin{bmatrix} \bar{\boldsymbol{R}}_{ve}^{II} & \bar{\boldsymbol{R}}_{ve}^{IQ} \\ \bar{\boldsymbol{R}}_{ve}^{QI} & \bar{\boldsymbol{R}}_{ve}^{QQ} \end{bmatrix}$$

$$\hat{\boldsymbol{R}}_{ve} = \begin{bmatrix} \hat{\boldsymbol{R}}_{ve}^{II} & \hat{\boldsymbol{R}}_{ve}^{IQ} \\ \hat{\boldsymbol{R}}_{ve}^{QI} & \hat{\boldsymbol{R}}_{ve}^{QQ} \end{bmatrix}$$

$$\boldsymbol{R}_{ve}^{ab} = \begin{bmatrix} r_{ve}^{ab}(0) & r_{ve}^{ab}(1) & \cdots & r_{ve}^{ab}(K-1) \\ r_{ve}^{ab}(1) & r_{ve}^{ab}(0) & \cdots & r_{ve}^{ab}(K-2) \\ \vdots & \vdots & & \vdots \\ r_{ve}^{ab}(K-1) & r_{ve}^{ab}(K-2) & \cdots & r_{ve}^{ab}(0) \end{bmatrix}.$$

$$\bar{\boldsymbol{R}}_{ve}^{ab} = \begin{bmatrix} r_{ve}^{ab}(0) & r_{ve}^{ab}(1) & \cdots & r_{ve}^{ab}(L-1) \\ r_{ve}^{ab}(1) & r_{ve}^{ab}(0) & \cdots & r_{ve}^{ab}(L-2) \\ \vdots & \vdots & & \vdots \\ r_{ve}^{ab}(L-1) & r_{ve}^{ab}(L-2) & \cdots & r_{ve}^{ab}(0) \end{bmatrix}.$$

$$\hat{\boldsymbol{R}}_{ve}^{ab} = \begin{bmatrix} & r_{ve}^{ab}(L) & r_{ve}^{ab}(L-1) & \cdots & r_{ve}^{ab}(K-1) \\ \bar{\boldsymbol{R}}_{ve}^{ab} & r_{ve}^{ab}(L-1) & r_{ve}^{ab}(L-2) & \cdots & r_{ve}^{ab}(K-2) \\ & \vdots & \vdots & & \vdots \\ & r_{ve}^{ab}(1) & r_{ve}^{ab}(2) & \cdots & r_{ve}^{ab}(K-L) \end{bmatrix}.$$

and a, bÏt$\{I, Q\}$.Now that we have the cost function expressed in terms of the second order statistics of the training and verification signals, we find the B that minimizes the cost function in 3.38. Differentiating 3.38 with respect to B [34], and equating to zero gives,

$$\bar{\boldsymbol{R}}_{ve}\boldsymbol{B}\boldsymbol{h}\boldsymbol{h}^H = \hat{\boldsymbol{R}}_{ve}\boldsymbol{h}\boldsymbol{h}^H. \tag{3.39}$$

One solution to 3.39 is

$$\boldsymbol{B} = \bar{\boldsymbol{R}}_{ve}^{-1}\hat{\boldsymbol{R}}_{ve},$$

or in other words, from 3.35

$$\bar{\boldsymbol{R}}_{tr}^{-1}\hat{\boldsymbol{R}}_{tr} = \bar{\boldsymbol{R}}_{ve}^{-1}\hat{\boldsymbol{R}}_{ve},$$

To satisfy the above we can choose

$$\bar{\boldsymbol{R}}_{tr} = \bar{\boldsymbol{R}}_{ve}$$

$$\hat{\boldsymbol{R}}_{tr} = \hat{\boldsymbol{R}}_{ve}$$

i.e., we choose the real and imaginary parts of $z_t r(n)$ and $z_v e(n)$ to have the same second-order statistics. Equivalently, the complex signals must have the same PSD.

Therefore, in this thesis, a training signal is carefully devised to mimic the spectral shape of a pre-distorted signal, and thus occupies the entire compensation bandwidth. This choice

of training signal provides higher SNR for the in-band portion than the conventional choice, thereby increasing the accuracy of the compensation filter coefficients in the in-band while still calibrating for the adjacent spectral bands. If a flat PSD over the target linearization bandwidth is adopted for the training signal, then the I/Q imbalance is estimated with equal accuracy over the entire band. Our choice of training signal decreases EVM with only a slight sacrifice in ACPR at the PA output after linearization as compared to the case where I/Q imbalance identification is conducted using a training signal with a flat PSD. This is advantageous as in mmWave communication applications, where the ACPR requirements are relaxed compared to EVM. To generate a training signal with the same PSD as that of a predistorted signal we use a memoryless polynomial. The order of the polynomial, P, is set so that it is the same as the order of the DPD that is to be used in the system. The coefficients, c_p, are also chosen to achieve similar ACPR to the PSD of the nonlinearity produced by the PA in the system. This ensures the PSD of the training signal comes as close as possible to the PSD of the signal it is being applied to without knowing the exact signal a priori, i.e.,

$$z_k(n) = \sum_{p=1}^{P} c_p u_k(n)|u_k(n)|^p. \tag{3.40}$$

In the above, $u_k(n)$ are independently generated OFDM signals. Therefore, the training signals,$z_k(n)$, for each transmitter are uncorrelated. In the next section, the performance increase of the proposed signal compared to that of the conventional signal is presented.

An example of the PSD of a training signal designed for I/Q compensation of a mmWave modulator is shown in Fig. 3.4. In this example, the PA non-linearity is assumed to generate spectral regrowth of 30 dBc below that of the in-band PSD. Thus, the training signal in Fig. 3.4 has an adjacent band PSD that is 30 dB below that of the in-band PSD. Fig. 3.4 also shows a conventional flat PSD training signal with identical total power.

3.3 Simulation and Measurement Results

In this section, we examine the performance of the concurrent I/Q imbalance compensation method using a single TOR. We show that the concurrent compensation method maintains

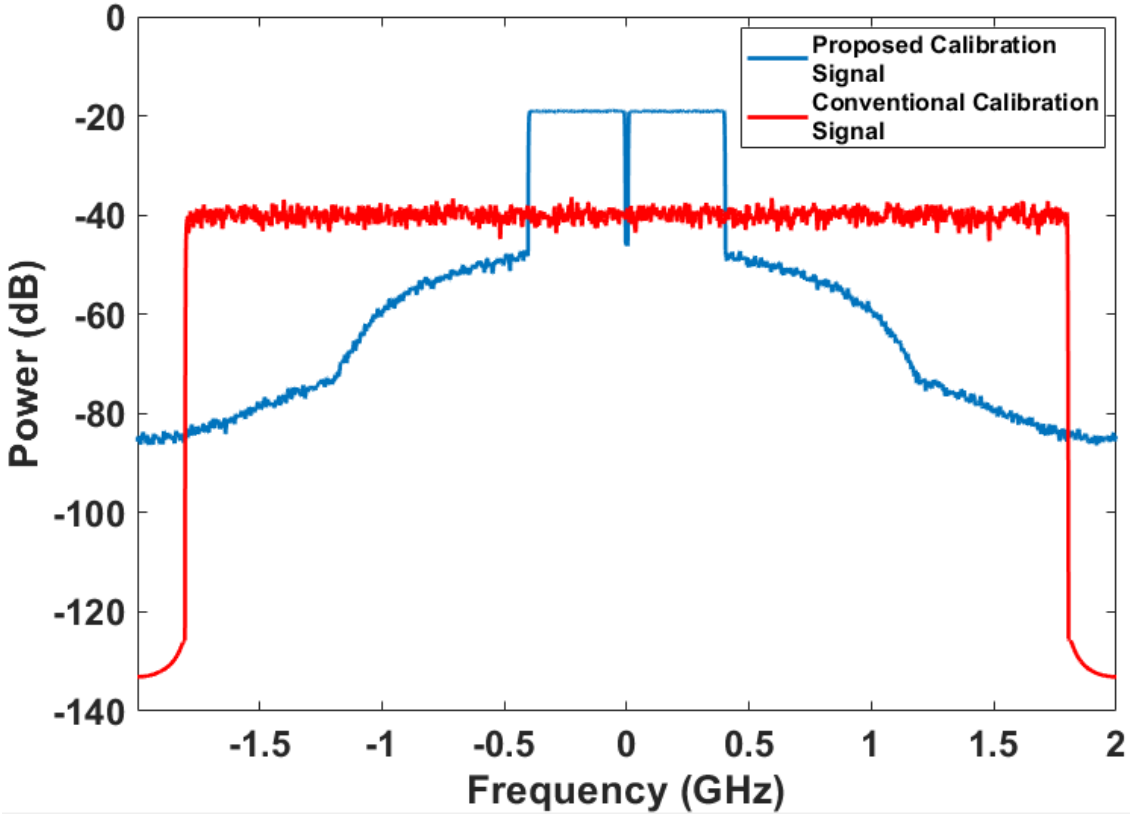

Figure 3.4: PSD of proposed training signal vs conventional training signal.

comparable performance to that of separate compensation, despite using a single TOR and reduced capture time. Moreover, we also compare the performance of the proposed training signal to the conventional signal with a flat PSD.

In order to validate the use of the proposed signal and the proof in the appendix, we use a 4GHz predistorted OFDM signal with an 800 MHz in-band bandwidth and 30dB ACPR for verification. Therefore we use NMSE as a measure of performance as opposed to EVM. EVM cannot be used because when the verification signal is generated, it is done so by using 3.30. Therefore if we were to calculate EVM using the original 800 MHz OFDM signal as our reference the EVM measurement would include the nonlinear distortion products caused by the predistortion function in 3.30 used to generate the verification signal.

3.3.1 I/Q Simulation Results

The performance of the proposed I/Q imbalance identification and compensation method is evaluated through simulation of four different large-scale MIMO systems that contain K =1, 2, 4, and 8 transmitters. The simulations were done in Keysight ADS. The simulation workbench for 4 transmitters can be seen in Fig. 3.5 For each system, nonlinear device models of MLIQ-1845L quadrature modulators provided by Marki microwave are used. The use of nonlinear device models suggests that much of the residual NMSE is due to nonlinear distortion of the signal. The output of each quadrature modulator is summed using both ideal Wilkinson power combiners and the s-parameters of physical quadrature modulators used in the measurement section. Using Data access components to upload custom signals to the quadrature modulators. Next, the proposed I/Q imbalance method is used to identify the corresponding 60-tap compensation filters. Then, the NMSE of the output of the quadrature modulator after compensation is used to assess the accuracy of the filters in compensating for the I/Q imbalance. The performance of the I/Q compensation is evaluated for the proposed training signal and the conventional signal with a flat PSD. The verification is performed with a 4GHz predistorted OFDM signal with an 800 MHz in-band bandwidth and 30 dB ACPR.

Table 3.1: I/Q Imbalance Simulation Results Reporting Mean NMSE for 1,2,4 and 8 Transmitters in % Before and After Compensation Using Both the Conventional Training Signal and the Proposed Training Signal and a 4GHz Predistorted Signal for Verification using Ideal Wilkinson Power Combiners and S-parameters of a Physical Wilkinson Power Combiner

Training Signal	4GHz Flat	4GHz Predistorted		
Transmitter Chains	1 Tx	1 Tx	2 Tx	4 Tx
NMSE Before Comp.	17.8	17.8	17.8	17.8
Ideal Wilkinson	2.13	1.22	1.22	1.22
Non-Ideal Wilkinson	2.13	1.22	2.21	3.30

The verification results are presented in Table 3.1. According to Table 3.1, with ideal combining, the proposed concurrent I/Q imbalance compensation method using a single

TOR achieved the same mean compensation accuracy for MIMO systems containing 1Table 3.1, 2, 4 and 8 transmitters. The application of their compensation filter allowed for the reduction of the mean NMSE from 17.8% to 1.22%Ḣowever, from row 3 in Table 3.1 we can see a progressive decrease in performance using the s-parameters of physical Wilkinson power combiners. This is due to the lack of isolation between the ports which is compounded by increasing the number of Wilkinson power combiners. From simulation, we find that the performance of the I/Q compensation method can be brought closer to that of Table 3.1 if the isolation between the Wilkinson power combiner ports is kept below the realistic value of -20 dB, compared to the current -11.0dB (combination of S(2,1), S(3,1) and S(4,1)) and -17.5dB for 4Tx and 2Tx, respectively.

In addition, from Table 3.1, it can be seen that the proposed training signal offers better performance than that of the conventional training signal. Also, as shown in Table 3.1, these results are very close to those obtained using a dedicated observation receiver for each transmitter channel and also match the measurement results presented in the next section.

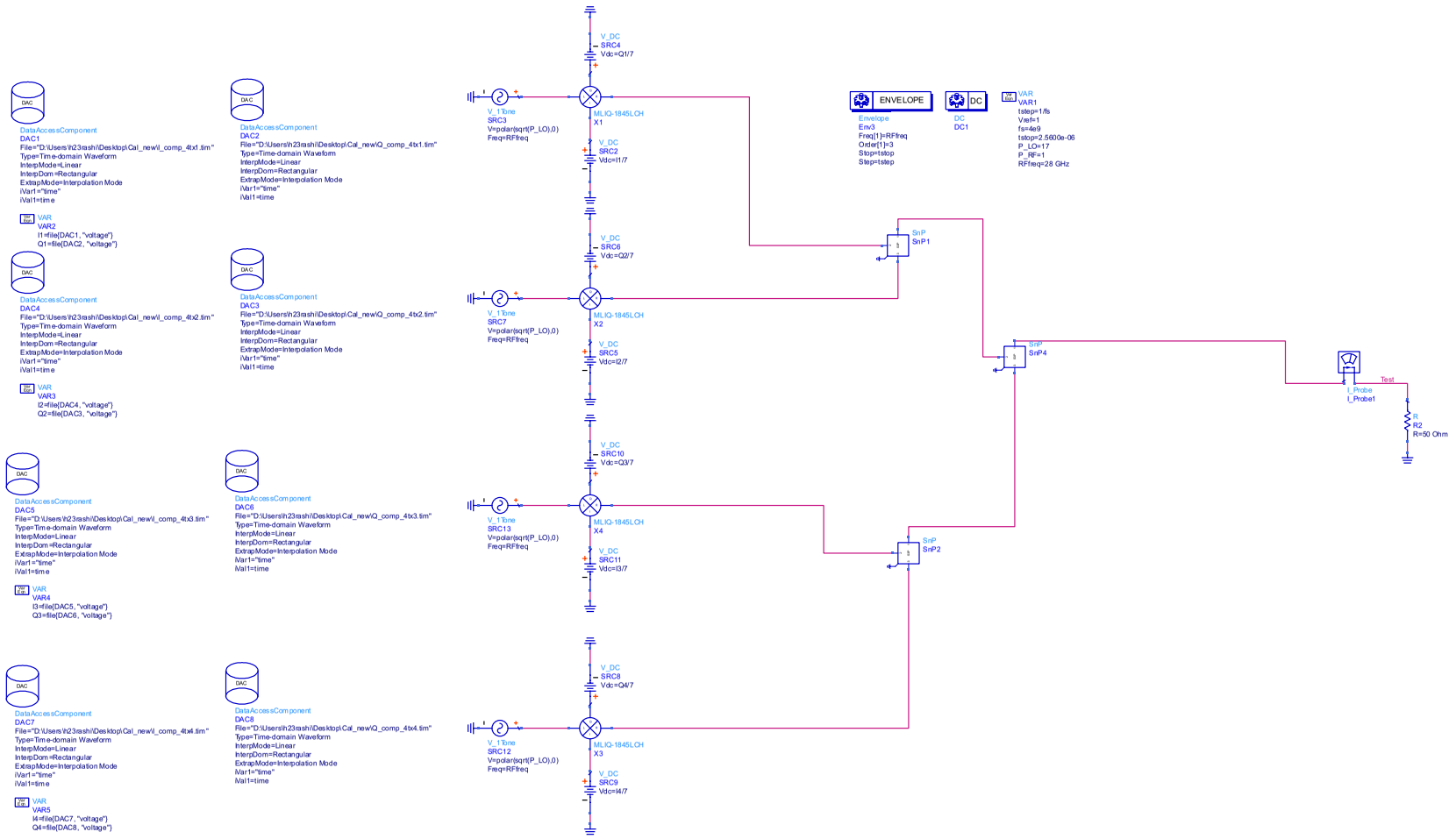

Figure 3.5: Simulation workbench for the simulated verification of the proposed concurrent I/Q imbalance identification and compensation scheme for four transmitter chains.

3.3.2 I/Q Measurement Results

In the following section, the proposed I/Q imbalance identification and compensation method is evaluated using the test setup shown in Fig. 3.6. In this setup, the I and Q components of four independent signals are generated using four arbitrary waveform generators (M8190A from Keysight Technology). These signals are fed to two I/Q mixers (MLIQ-1845 from Marki) for quadrature modulation. The LO signals are generated using two analog signal generators (N5183B from Keysight Technology). The RF signals at the output of the four I/Q mixers, $y_1(t)$, $y_2(t)$, $y_3(t)$ and $y_4(t)$ are centered at 28GHz. These four signals are then combined using three Wilkinson power combiners (two PD-0434SM and one PD-0140 from Marki) to yield the feedback signal needed to identify the I/Q imbalance of the two I/Q mixers. This feedback signal is first fed to the down conversion mixer (MM1-1140H from Marki). The LO signal needed by the down-conversion mixer is generated using a signal generator (HMC-T2240 from Hittite). The intermediate frequency signal, centered around 3 GHz, is subsequently captured using a 10-bit 8GHz bandwidth high-speed oscilloscope (MSOS804A from Keysight Technology).

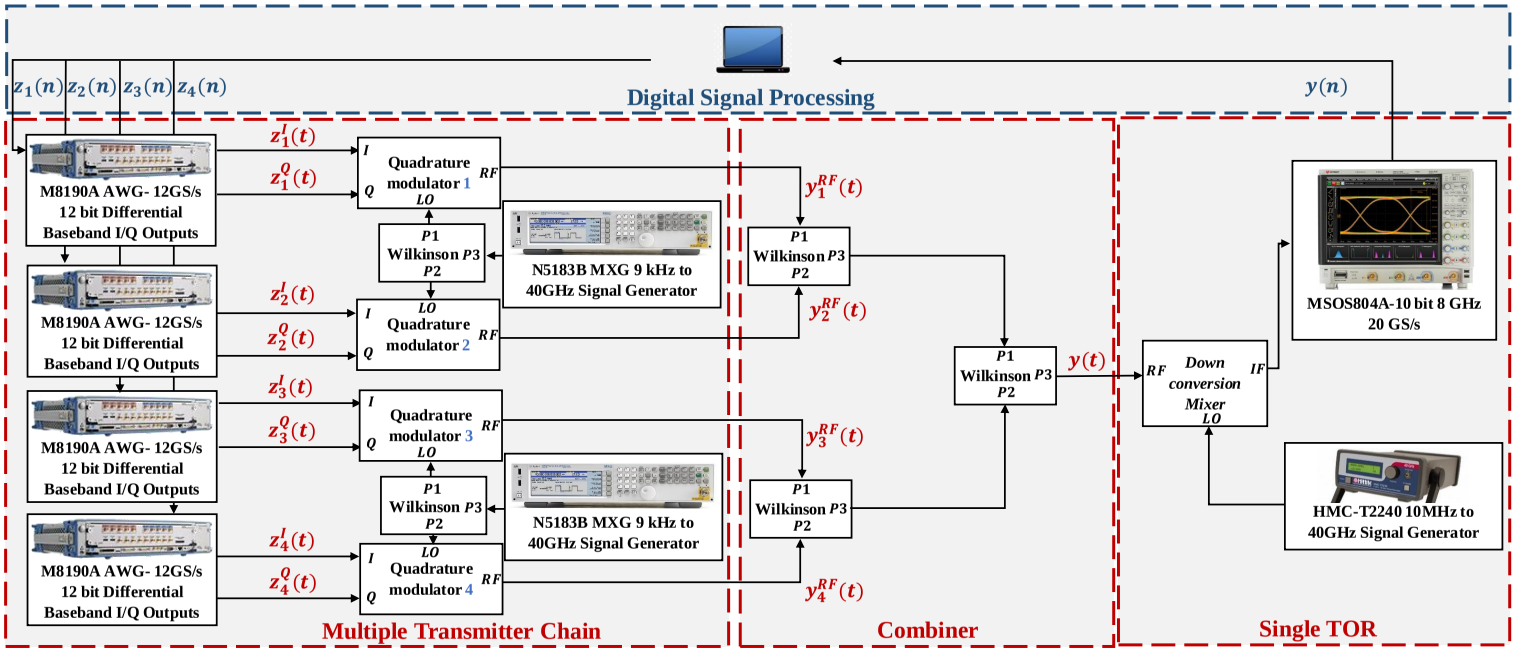

Figure 3.6: Test setup for the experimental verification of the proposed concurrent I/Q imbalance identification and compensation scheme for four transmitter chains.

Table 3.2: I/Q Imbalance Measurement Results Reporting NMSE for 1,2 and 4 Transmitters in % Before and After Compensation Using Both the Conventional Training Signal and the Proposed Training Signal and a 4GHz Predistorted Signal for Verification

Training Signal	4GHz Flat	4GHz Predistorted		
Transmitter Chains	1 Tx	1 Tx	2 Tx	4 Tx
NMSE Before Comp.	19.0	19.0	19.0	19.0
NMSE After 20-tap	3.86	2.36	2.53	3.98
NMSE After 60-tap	3.39	1.99	2.25	3.39
NMSE After 120-tap	3.36	1.63	2.16	3.29

The performance of the concurrent compensation for 2 and 4 transmitter chains enabled simultaneously is then compared to that of separate compensation, whereby all chains but one are turned off and the performance of the single chain is examined independently of all other transmitters. This is done with both the conventional and proposed training signals. Here, the capture time of the concurrent method is fixed to be the same as that for compensation of a single transmitter chain in the sequential method. In other words, for K transmitter chains, the proposed method requires K times less capture time.

The result from this verification experiment are summarized in Table 3.2. In the case of separate compensation, compared to using the conventional training signal, the proposed training signal allowed for significant improvement in accuracy. For example, I/Q compensation filters, for 2Tx, with 60 taps allowed for the NMSE of 19.0% to be reduced to 2.25% . Furthermore, the increase of the number of taps from 20 to 60 per filter further improved the accuracy in the case of the proposed training signal, yet only incremental improvements were observed for the conventional training signal. In addition, according to Table 3.2, the proposed concurrent identification and compensation method for 2 and 4 transmitters maintains comparable performance to that of separate compensation, despite using a single TOR and reduced capture time. As predicted by the trend shown in simulations, there is a small reduction in performance caused by the lack of isolation between the ports of the Wilkinson power combiners. This could be alleviated if the isolation between the ports was reduced from the current [number]dB to [number]dB as confirmed by the

simulations.

3.3.3 DPD Measurement Results

Finally, to assess the improved accuracy of the I/Q imbalance identification and compensation that can be attributed to the choice of the training signal, we combine I/Q imbalance identification with DPD for linearizing a PA. Specifically, we compare the linearization performance when using the cascade of an I/Q mixer and a mmWave PA where the I/Q imbalance identified using the conventional or the proposed training signal in back-off, and the PA is linearized using a complexity-reduced Volterra (CRV) DPD model [18]. This experiment is conducted with a mmWave PA (HMC1131 from Analog Devices) and with 60-tap compensation filters. Furthermore, the CRV model is chosen with parameters as follows: the non-linearity order is $N = 7$, while the linear memory depth is $M_L = 20$, and the non-linear memory depth is $M_{NL} = 9$. Table 3.3 summarizes the results of the DPD linearization. From Table 3.3, we can see significant improvement in EVM with and without a compensation filters. Moreover, we can see that we gain significant performance in EVM (1.2%) with only a 1dB sacrifice in ACPR when comparing to the results obtained using conventional training signals for I/Q imbalance identification.

Table 3.3: DPD Linearization Measurement Results Reporting EVM in % for a mmWave PA Using an 800MHz OFDM Signal.

Training Signal	No DPD and No I/Q Comp.	DPD and No I/Q Comp.	DPD and Conv. I/Q Comp.	DPD and Proposed I/Q Comp.
NMSE	24.4%	17.20%	2.0%	0.86%
ACPR (L/U) (dBc)	35/35	40/40	49/49	48/49

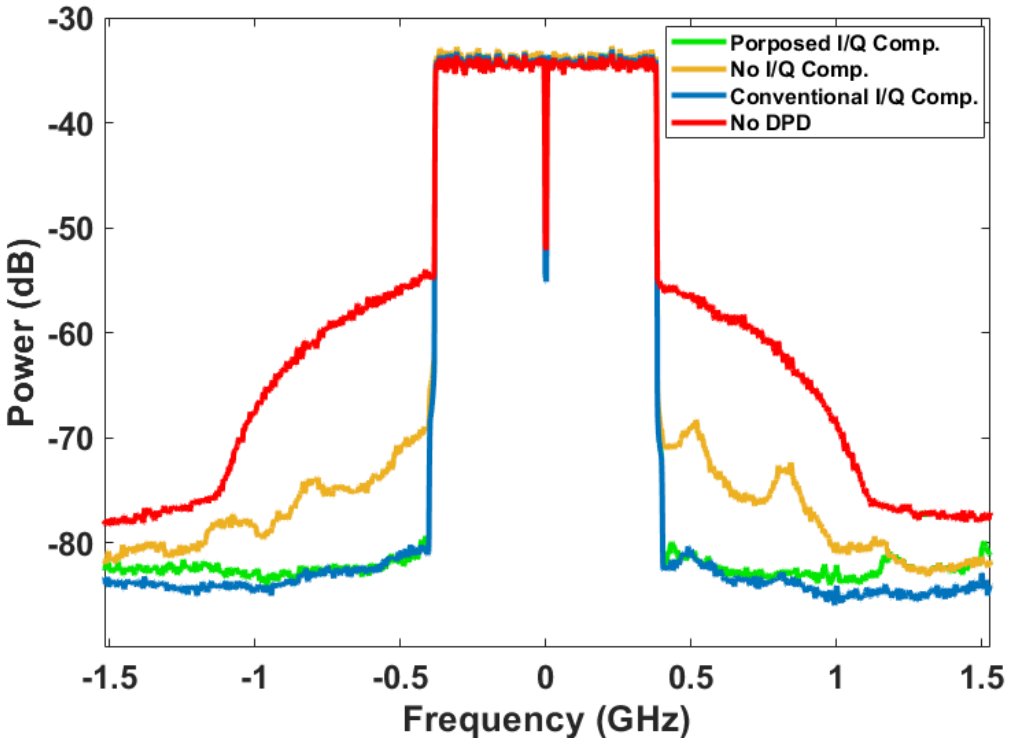

Figure 3.7: Measured spectra of DPD with and without I/Q imbalance compensation.

Chapter 4

Conclusion

In this thesis, we proposed a method to concurrently identify and compensate the I/Q imbalance in mm-wave MIMO direct-conversion Tx using a single TOR that captures the combined output of all chains. The proposed I/Q imbalance identification and compensation method was validated using a 4 GHz predistorted OFDM signal with an 800 MHz in-band and 30 dB ACPR in simulation for 1, 2, 4 and 8 Tx chains as well as in measurement using a custom built transmitter comprised of 1, 2 and 4 mm-wave Tx chains utilizing commercially available quadrature modulators. For 2 Tx with 60-taps, the concurrent compensation method obtained NMSEs of 19% before and 2.25% after I/Q imbalance compensation.This thesis also proves in simulation and in measurement that judiciously engineered uncorrelated training signals with the same PSD as the predistorted signal generated by DPD are optimal for minimizing the EVM while maintaining low ACPR in the out-of-band region when applying DPD. These types of training signals would be optimal for new 5G standards where mmWave transmitters have strict EVM requirements; while ACPR requirements are relaxed. Finally, the compensation accuracy of the proposed method was further confirmed when the I/Q compensation filters are calculated in back-off and applied during the DPD linearization of a mm-wave PA.

4.1 Future Work

In future works, the theory in this thesis could simply be extended to compensate for the frequency response of any transmitter chain, whether or not it contained a quadrature modulator. This could be done by modeling the frequency response as one complex valued FIR filter, and continuing on as outlined in this thesis. This would be useful for systems where RFDACs generate the signal at IF, which is then up-converted to RF frequencies by a mixer. As a second extension, a concurrent MIMO DPD compensation method could be used in conjunction with this I/Q imbalance compensation method where the I/Q compensation filters are trained in back-off.

References

[1] T. S. Rappaport, S. Sun, R. Mayzus, H. Zhao, Y. Azar, K. Wang, G. N. Wong, J. K. Schulz, M. Samimi, and F. Gutierrez, "Millimeter wave mobile communications for 5g cellular: It will work!" *IEEE Access*, vol. 1, pp. 335–349, 2013.

[2] K. C. Amy Nordrum and I. S. Staff, "Everything you need to know about 5g," Available at https://spectrum.ieee.org/video/telecom/wireless/everything-you-need-to-know-about-5g (2017).

[3] 3GPP, "Technical specification group radio access network;nr; base station (bs) radio transmission and reception," Valbonne, France, Tech. Rep., 2019.

[4] E. G. Larsson, O. Edfors, F. Tufvesson, and T. L. Marzetta, "Massive mimo for next generation wireless systems," *IEEE Communications Magazine*, vol. 52, no. 2, pp. 186–195, February 2014.

[5] S. Han, C. I, Z. Xu, and C. Rowell, "Large-scale antenna systems with hybrid analog and digital beamforming for millimeter wave 5g," *IEEE Communications Magazine*, vol. 53, no. 1, pp. 186–194, January 2015.

[6] B. Razavi, *RF Microelectronics*, 2nd ed. Upper Saddle River, NJ , USA: Prentice Hall, 2011.

[7] R. Lyons, "A quadrature signals tutorial: Complex, but not complicated," Available at https://mriquestions.com/uploads/3/4/5/7/34572113/quad_signals_tutorial-lyons.pdf (2013).

[8] J. Cavers and M. Liao, "Adaptive compensation for imbalance and offset losses in direct conversion transceivers," *Vehicular Technology, IEEE Transactions on*, vol. 42, pp. 581 – 588, 12 1993.

[9] S. A. Bassam, S. Boumaiza, and F. M. Ghannouchi, "Block-wise estimation of and compensation for i/q imbalance in direct-conversion transmitters," *IEEE Transactions on Signal Processing*, vol. 57, no. 12, pp. 4970–4973, Dec 2009.

[10] Li Yu and W. M. Snelgrove, "A novel adaptive mismatch cancellation system for quadrature if radio receivers," *IEEE Transactions on Circuits and Systems II: Analog and Digital Signal Processing*, vol. 46, no. 6, pp. 789–801, June 1999.

[11] L. Ding, Z. Ma, D. R. Morgan, M. Zierdt, and G. T. Zhou, "Compensation of frequency-dependent gain/phase imbalance in predistortion linearization systems," *IEEE Transactions on Circuits and Systems I: Regular Papers*, vol. 55, no. 1, pp. 390–397, Feb 2008.

[12] A. Chung, M. Ben Rejeb, Y. Beltagy, A. M. Darwish, H. A. Hung, and S. Boumaiza, "Iq imbalance compensation and digital predistortion for millimeter-wave transmitters using reduced sampling rate observations," *IEEE Transactions on Microwave Theory and Techniques*, vol. 66, no. 7, pp. 3433–3442, July 2018.

[13] L. Anttila, M. Valkama, and M. Renfors, "Frequency-selective i/q mismatch calibration of wideband direct-conversion transmitters," *IEEE Transactions on Circuits and Systems II: Express Briefs*, vol. 55, no. 4, pp. 359–363, April 2008.

[14] L. Anttila, P. Handel, and M. Valkama, "Joint mitigation of power amplifier and i/q modulator impairments in broadband direct-conversion transmitters," *IEEE Transactions on Microwave Theory and Techniques*, vol. 58, no. 4, pp. 730–739, April 2010.

[15] L. Fan, Y. Li, and M. Zhao, "Joint iq imbalance and pa nonlinearity pre-distortion for highly integrated millimeter-wave transmitters," in *2014 IEEE Globecom Workshops (GC Wkshps)*, Dec 2014, pp. 399–404.

[16] Y. Li, C.-F. Cheang, P.-I. Mak, and R. P. Martins, "Joint-digital-predistortion for wireless transmitter's i/q imbalance and pa nonlinearities using an asymmetrical complexity-reduced volterra series model," *Analog Integrated Circuits and Signal Processing*, vol. 87, no. 1, pp. 35–47, Apr 2016. [Online]. Available: https://doi.org/10.1007/s10470-016-0724-2

[17] L. Ding, "Digital predistortion of power amplifiers for wireless applications," Ph.D. dissertation, School of Elect. and Comp. Eng., Georgia Tech., Atlanta, GA, USA, 2004.

[18] M. C. F. S. Boumaiza, F. Mkadem and J. Wood, "Complexity reduced volterra series model for power amplifier digital predistortion," *Analog Integr. Circuits Signal Process.*, vol. 79, pp. 331–343, Feb. 2014.

[19] M. Marcus and B. Pattan, "Millimeter wave propagation: spectrum management implications," *IEEE Microwave Magazine*, vol. 6, no. 2, pp. 54–62, June 2005.

[20] W. Roh, J. Seol, J. Park, B. Lee, J. Lee, Y. Kim, J. Cho, K. Cheun, and F. Aryanfar, "Millimeter-wave beamforming as an enabling technology for 5g cellular communications: theoretical feasibility and prototype results," *IEEE Communications Magazine*, vol. 52, no. 2, pp. 106–113, February 2014.

[21] A. Gupta and R. K. Jha, "A survey of 5g network: Architecture and emerging technologies," *IEEE Access*, vol. 3, pp. 1206–1232, 2015.

[22] I. Ahmed, H. Khammari, A. Shahid, A. Musa, K. S. Kim, E. De Poorter, and I. Moerman, "A survey on hybrid beamforming techniques in 5g: Architecture and system model perspectives," *IEEE Communications Surveys Tutorials*, vol. 20, no. 4, pp. 3060–3097, Fourthquarter 2018.

[23] F. Sohrabi and W. Yu, "Hybrid digital and analog beamforming design for large-scale antenna arrays," *IEEE Journal of Selected Topics in Signal Processing*, vol. 10, no. 3, pp. 501–513, April 2016.

[24] S. Han, C. I, Z. Xu, and C. Rowell, "Large-scale antenna systems with hybrid analog and digital beamforming for millimeter wave 5g," *IEEE Communications Magazine*, vol. 53, no. 1, pp. 186–194, January 2015.

[25] C. Masterson, "Massive mimo and beamforming: The signal processing behind the 5g buzzwords," Limerick, Ireland, Tech. Rep., June 2017.

[26] P. Jaraut, M. Rawat, and F. M. Ghannouchi, "Composite neural network digital predistortion model for joint mitigation of crosstalk,i/qimbalance, nonlinearity in mimo transmitters," *IEEE Transactions on Microwave Theory and Techniques*, vol. 66, no. 11, pp. 5011–5020, Nov 2018.

[27] Z. A. Khan, E. Zenteno, P. HÃďndel, and M. Isaksson, "Digital predistortion for joint mitigation of i/q imbalance and mimo power amplifier distortion," *IEEE Transactions on Microwave Theory and Techniques*, vol. 65, no. 1, pp. 322–333, Jan 2017.

[28] A. Tarighat and A. H. Sayed, "Joint compensation of transmitter and receiver impairments in ofdm systems," *IEEE Transactions on Wireless Communications*, vol. 6, no. 1, pp. 240–247, Jan 2007.

[29] Q. Zou, A. Tarighat, and A. H. Sayed, "Joint compensation of iq imbalance and phase noise in ofdm wireless systems," *IEEE Transactions on Communications*, vol. 57, no. 2, pp. 404–414, February 2009.

[30] O. Ozdemir, R. Hamila, and N. Al-Dhahir, "I/q imbalance in multiple beamforming OFDM transceivers: Sinr analysis and digital baseband compensation," *IEEE Transactions on Communications*, vol. 61, no. 5, pp. 1914–1925, May 2013.

[31] J. K. Cavers, "The effect of quadrature modulator and demodulator errors on adaptive digital predistorters for amplifier linearization," *IEEE Transactions on Vehicular Technology*, vol. 46, no. 2, pp. 456–466, May 1997.

[32] A. H. Sayed, *Adaptive Filters*. Hoboken, NJ, USA: John Wiley & Sons, 2008.

[33] P. Ramabadran, S. Madhuwantha, P. Afanasyev, R. Farrell, L. Marco, S. Pires, and J. Dooley, "Digitally assisted wideband compensation of parallel rf signal paths in a

transmitter," in *2018 91st ARFTG Microwave Measurement Conference (ARFTG)*, June 2018, pp. 1–4.

[34] K. B. Peterson and M. S. Pedersen, *The Matrix Cookbook*, 2012 ed. Waterloo, ON, CAN: University of Waterloo, 2012.

[35] E. BjÃűrnson, J. Hoydis, M. Kountouris, and M. Debbah, "Massive mimo systems with non-ideal hardware: Energy efficiency, estimation, and capacity limits," *IEEE Transactions on Information Theory*, vol. 60, no. 11, pp. 7112–7139, Nov 2014.

[36] S. M. Kay, *Fundamentals of Statistical Processing, Volume I: Estimation Theory*, 1st ed. Upper Saddle River, NJ , USA: Prentice Hall, 1993.